CHALMERS

Neural Signal Processing of Microelectrode Recordings for Deep Brain Stimulation

Xuan He

Signal Processing Group
Department of Signals and Systems

Chalmers University of Technology

Master Thesis

Neural Signal Processing of Microelectrode Recordings for Deep Brain Stimulation

Xuan He

hexuan.hx@gmail.com

2009/11/25

Table of Content

Abstract

Microelectrode Recording (MER) that can measure the activity from individual neurons is a popular method for target nucleus localization used during deep brain stimulation for Parkinson Disease (PD). Currently, MER assessment is performed by experienced neurologists during the surgery by analyzing the audio and visual conversions of the MER signal. The process of MER signal assessment could increase the patients' burden since patients are awake during the surgery.

In this thesis, an automated localization algorithm was developed, which could provide reliable and fast target nucleus localization. Firstly, MER signal was separated into: background noise, action potentials and artifacts. Then the best indicators were chosen for developing the targeting algorithm by extracting multiple computational features and comparing the performance among them. The tests were performed afterwards to validate the efficacy of the resulting algorithm. The overall result was that 89% agreement level was achieved from the comparison between the annotations from automated algorithm and three independent neurologists' annotations.

Keywords: Deep brain stimulation, microelectrode recording, signal components separation, feature extraction, threshold detection, target localization.

Acknowledgement

First of all, I want to thank all of my supervisors at Philips Research in Eindhoven: Dr. Kevin Dolan, Hayriye Cagnan and Dr. Hubert Martens. Thanks very much for giving me the opportunity to do this master work at Philips Research. I have learned a lot during the past 9 months. Neural science was a totally new field to me at beginning of my thesis work. So I am really appreciated the detailed guidance, the warm encouragement, the fully support and the helpful suggestions from all of you. Besides, you also taught me how to logically organize the work and deliver the result efficiently. Without your help, my thesis work can never reach this point.

Secondly, I would like to thank Dr. Lo Bour and MD. Maria Fiorella Contarino from Academic Medical Centre in Amsterdam. Thanks very much for providing all the helpful information for my thesis work and also letting me to join the discussion meeting and also visit the surgery, which helps me to have a deeper understanding of the whole project.

Moreover, I appreciated all the help from Prof. Mats Viberg, my examiner from Chalmers University of Technology. Thanks very much for giving me useful suggestions during my thesis work and helping me to revise my thesis report.

Last but not least, thanks very much for all the help, support and encouragement from my family and friends. You made me strong enough to confront all the difficulties for my days away from home.

Thank you very much!

Abbreviations

PD: Parkinson Disease

DBS: Deep Brain Stimulation

MER: Microelectrode Recording

STN: Subthalamic Nucleus

SN: Substantia Nigra

AC: Anterior Commissure

PC: Posterior Commissure

SNc: Substantia Nigra Pars Compacta

GPe: Globus Pallidus External

GPi: Globus Pallidus Internal

ISI: Inter Spike Interval

MBI: Modified Burst Index

CL: Curve Length

ANE: Average Nonlinear Energy

AAD: Average Absolute Difference

PR: Pause Ratio

PI: Pause Index

TI: Tonic Index

PS: Poisson Surprise

ISI rms: the standard deviation of interspike interval

Preface

This is a master thesis report for the master program Communication Engineering at Chalmers University of Technology. The thesis work was performed at Philips Research in Eindhoven, Netherlands from 2009-03-01 to 2009-11-30. The objective of this thesis work is to develop an automated target localization algorithm for the Deep Brain Stimulation) neurosurgery.

This report is organized in the following way:

In chapter 1, the necessary background information for this thesis work is introduced regarding the pathology of Parkinson Disease (PD), Deep Brain Stimulation (DBS) and the basic concept of microelectrode recordings (MER). The objective and the work flow of this thesis are also briefly described.

The following chapters are the detailed descriptions of the processing and analysis of the MER signal. In chapter 2, according to thesis work flow, background noise level estimation is applied to the raw MER signal using three different methods. Then, artifact rejection and spike detection algorithm are performed with respect to the estimated noise level.

In chapter 3, multiple computational features are introduced separately for the purpose of target nucleus localization. The feature extraction is applied on several types of transformed MER signals. Good features that can indicate the locations of brain structures, like subthalamic nucleus (STN) and substantia Nigra (SN) will then be chosen for developing the target localization algorithm.

Chapter 4 describes the automated target localization algorithm. Following the development of the targeting algorithm, the test and the analysis of the resulting algorithm are applied.

The conclusion and possible future work are presented in Chapter 5.

Chapter 1 Background Information

1.1 Parkinson Disease

1.1.1 Pathology of Parkinson Disease

Parkinson Disease (PD) is a chronic and progressive disease. This disease belongs to the group of movement disorders, which mostly happens among people older than 60 years old. The specific causes of PD remain unknown and the symptoms of PD are varying from patient to patient. However, tremor, rigidity, bradykinesia and postural instability are considered as four cardinal symptoms for this disease[1]. Tremor describes a rhythmic and involuntary muscle movement. Rigidity refers to the resistance to passive movement of the patients. As to bradykinesia, it is defined as the slowness of PD patients' movement. And postural instability, which usually appears in the late stages of PD, means that the movements of PD patients are not stable, so they have poor balance and may easily fall.

The basal ganglia area of the brain has become an interesting region to study due to clinical observations of PD and other kinds of movement disorders disease. The basal ganglia area consists of following interconnected nuclei: the striatum that composed of two nuclei caudate and putamen, the external and internal segments of globus pallidus (GPe & GPi), subthalamic nucleus (STN), and substantia Nigra (SN)[2]. The relative locations of these nuclei are shown in Figure 1.1.
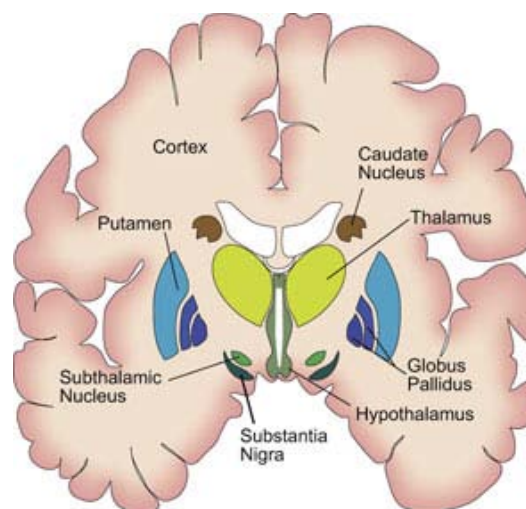
Figure 1.1 The Basal Ganglia area. Main nuclei within the Basal Ganglia area of the brain are: striatum, GPe, GPi, STN and SN. (Figure adapted from [3].)

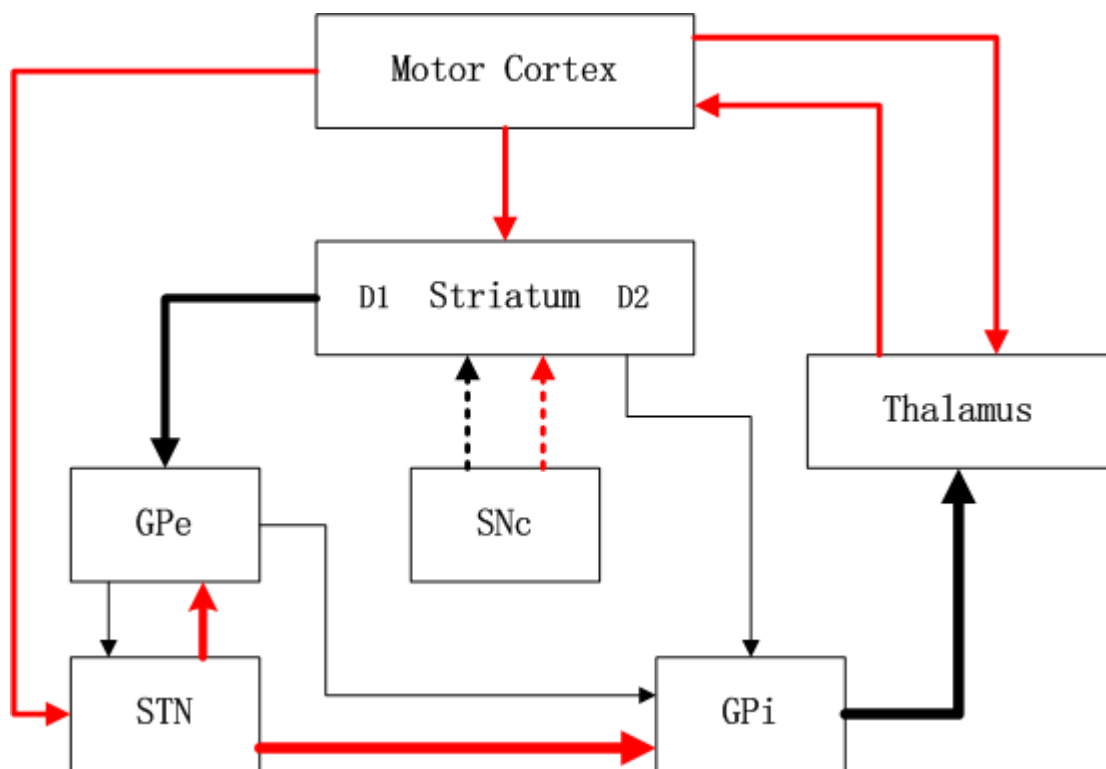The signal transmission for movement control could be seen as a closed circuit (Figure 1.2). Functionally, the basal ganglia nuclei take part in excitating and inhibiting movement, controlling the action selection and timing issues. The output of basal ganglia projects onto the thalamus, which in turn projects to the cortex (the highest processing center in the brain).
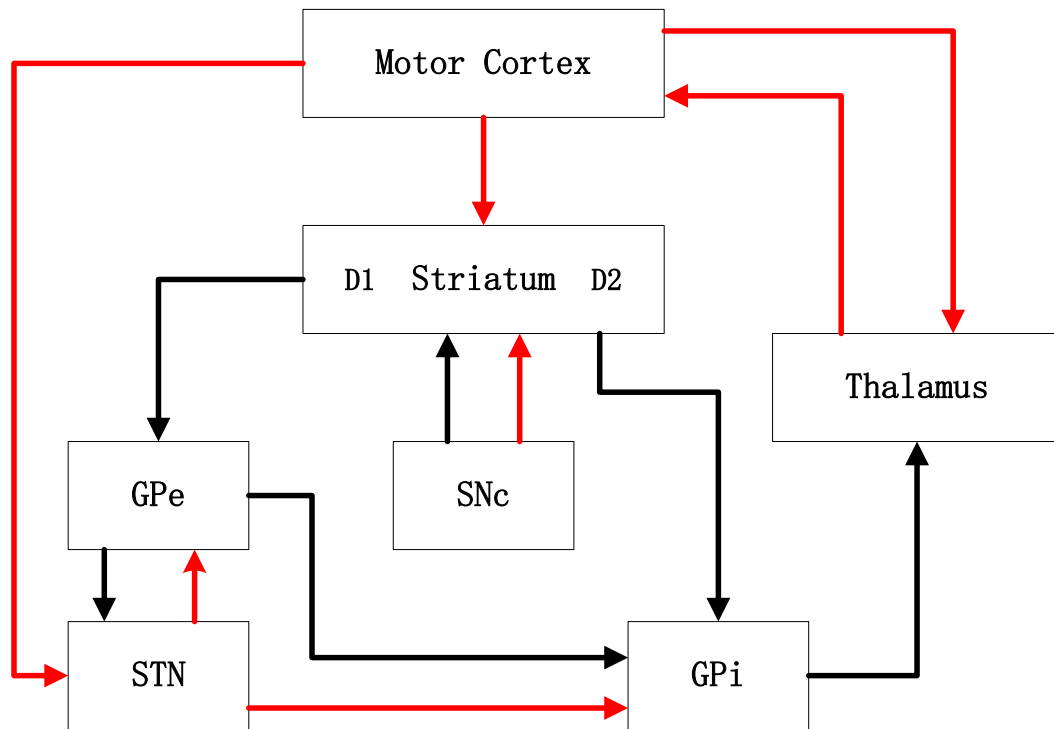
Figure 1.2 Neural network for movement control (normal). Neural Signal Transmission for Movement Control is started from the nucleus SNc, the output projects to striatum, which then goes via direct and indirect ways to GPi. After that, the Output signal from GPi delivers to thalamus that direct communicates with Motor Cortex.

Substantia nigra pars compacta (SNc) is a portion of SN. The transmitted signal from SNc projects to striatum at first. Then at striatum, the dopaminergic input from the SNc affects two dopamine receptors D1 and D2, respectively. The transmitted signal excites D1 receptors, but inhibits D2 receptors. After that, the output of the striatum projects to the GPi via two links. One is the "direct pathway" that excites movement. The other is "indirect pathway" that inhibits transmission from the striatum to the GPe. The output signal from GPi will project to thalamus and communicates with cortex directly.

For a PD patient, the dopaminergic neurons degenerate in the SNc. Because of this, the signal transmission though both the direct and indirect pathways are altered in PD patients when compared with the healthy people. In the direct pathway, the inhibition signal projected from striatum to GPi reduces, which then leads to the decrease of inhibition of neural activity in the GPi. On the other hand, in the indirect pathway, the inhibition signal from GPe to GPi decreases and at the same time the excitation signal from STN to GPi increases. The signal transmitted both in the direct and indirect pathways lead to the hyper-activity in the GPi. The consequences are the increased inhibition signal in the thalamus, which finally inhibits the control of voluntary movement through the projections from thalamus to motor cortex[4]. Moreover the imbalanced signal transmission in the direct and indirect pathways also leads to a synchronized oscillatory neuronal activity in the basal ganglia area within the frequency ranged from 3 to 30Hz[5]. Figure 1.3 shows the abnormal neural signal transmission in a PD patient.

Figure 1.3 Neural network for movement control (PD patient). Neural Signal Transmission in a PD patient is different from Figure 1.2 (neural signal transmission for healthy brain). Due to the dopaminergic neurons degeneration in SNc, the signal transmission in both direct and indirect ways changed. The hyper-active signal in GPi finally leads to the increasing inhibition signal back to cortex.

1.1.2 Treatment for Parkinson Disease

At the beginning stage of PD, when dopamine starts to degenerate in the SNc, the brain can dynamically adapt to its loss through compensating the movement control via other neuron signal transmission circuits within the brain. However, at the level that about 80% of dopaminergic neurons degenerated in the SNc, the cardinal symptoms of PD start to show up. Since pathological and synchronized neuronal activities of the affected nuclei result from the absence of dopamine within the basal ganglia area, the treatment for PD is either to improve the dopamine level in the basal ganglia or to disrupt the synchronization between these nuclei in order to retrieve their independent firing.

The medication treatment for PD is trying to improve the level of dopamine in the basal ganglia area on the brain. Levodopa is widely used for the treatment since it can transform into dopamine and reduces the effect of the SNc degeneration. However, levodopa does not only increase the concentration of dopamine within the basal ganglia area but also increase the dopamine level in the other brain areas and introduces some unwanted side-effects[1].

Treatment that can be considered at advanced stages of PD is neurosurgery. Lesion surgery is the earliest surgery that ablates several nuclei affected by the loss of dopaminergic neurons in the SNc. Specifically, the ablated nuclei are: STN, GPi or the thalamus. After lesioning, the symptoms of PD patients reduced dramatically. However, the procedure of lesioning may lead to potential damage to the neighboring brain structures and introduce unwanted side-effect. In 1950s, electrical stimulation was accidently applied during lesioning surgery and the reducing of the PD symptoms are observed without nuclei ablation, which on the other hand means it is much safer. As a result, electrical neuro stimulation surgery has gradually replaced the lesioning surgery. And this electrical neuro stimulation surgery is the so called Deep Brain Stimulation (DBS) [4].

1.2 Deep Brain Stimulation

Deep Brain Stimulation (DBS) is a neurosurgery to treat PD and other kinds of movement disorder diseases. By implanting a small electrode within the target nucleus, either the STN or the GPi in the basal ganglia area of the brain and then applying high frequency electrical stimulation at 130-185Hz [4], the pathological neural activities in the target nucleus could be altered.

Figure 1.4 Deep Brain Stimulation (DBS). For DBS surgery, an electrode is implanted in the brain for applying high frequency stimulation. The electrical impulse is delivered through wire connection from pulse generator that embedded under collar bone. ((Figure adapted from [6].)
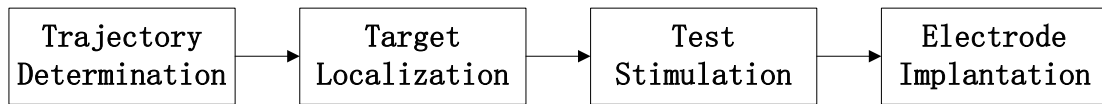
1.2.1 Mechanism of Deep Brain Stimulation

One hypothesis of DBS's action mechanism is that DBS acted as a functional lesion. With respect to the cardinal features of the movement disorders, lesioning and high frequency stimulation lead to similar clinical results. However, evidence later suggested that DBS stimulation not only suppress local neuronal activities but also increase the output from the stimulated target nucleus. Whether high frequency stimulation leads to the direct neuronal blockage or causes the activation of inhibitory elements has not been clarified, but it has been proved that the mechanism of DBS is more complicated than lesioning [4].

1.2.2 DBS Procedure

The procedure of DBS surgery is composed of two parts. The first part is the stereotactic neurosurgery that involves implanting a small electrode at the target location inside the brain. And the second part is to embed a pacemaker under the collarbone of the patient. The pacemaker connects to the electrode through a hair-thin wire. Thereby, it can deliver electrical impulses to the electrode to apply high frequency stimulation at target location. The surgical time spend on the first part for electrode implantation is around 6-8 hours, thus the second part often takes place on a different day.

As to the part of electrode implantation, the work flow is shown in Figure 1.5:

```
┌──────────────┐     ┌──────────────┐     ┌──────────────┐     ┌──────────────┐
│  Trajectory  │ ──▶ │    Target    │ ──▶ │     Test     │ ──▶ │   Electrode  │
│ Determination│     │ Localization │     │  Stimulation │     │ Implantation │
└──────────────┘     └──────────────┘     └──────────────┘     └──────────────┘
```

Figure 1.5 Electrode implantation work flow. Before DBS electrode implantation, there are three pre steps: trajectory determination, target localization and test stimulation.

The first step is trajectory determination. Before the surgery, the neurosurgical team first needs to determine a suitable trajectory and an estimated target point for electrode implantation. Trajectory is determined through visually analyzing the 3D medical images, such as MRI scan. With respect to the anatomical landmarks AC (the anterior commissure) and PC (the posterior commissure), a trajectory is planned which reduces the risk of penetrating any critical cerebral tissue. MR image also helps to give suggestion about the approximate estimated target nucleus STN, but it is not accurate enough because the STN is located in the gray matter regions of the deep brain, the size of it is very small, and the contrast of it is relatively poor compared with the surrounding structures on MR image. Moreover, the actual optimal location for applying high frequency electrical stimulation within STN varies from patient to patient for DBS surgery. Therefore, imaging alone cannot provide accurate target location and a more accurate localization method is needed, which is the necessary step after trajectory determination.

Electrophysiology is the most popular way to pursue accurate target localization. It is performed by MER. Nowadays, the experienced neurologists assess the MERs and indicate the target location during the surgery. More details about MER are presented in Chapter 1.3.

After accurate target localization, high frequency stimulation is applied at several locations within the target nucleus. This purpose of this step is to choose the target location for final implanting DBS electrode that can reduce the symptoms of PD without introducing any side effect.

1.3 Microelectrode Recording

The cellular membrane of a neuron acts as a capacitor. Through rapid transient changes of the membrane potential (action potential), neurons are able to transmit information by electrical means and generate extra cellular currents and electrical fields. By detecting and recording the electrical signals, microelectrode can measure the neuron activity from individual neurons within 100 to 200 microns.

The tool for microelectrode recording (MER) is a microelectrode needle with tiny probes, which can measure the action potentials from individual neurons within the local vicinity of the probe tips. Usually, five probes are placed about 2mm away from each other in a 'diamond pattern'. According to anatomical directions (Figure 1.6), the recordings we got correspond to five probes are named with central, medial, lateral, anterior and posterior.
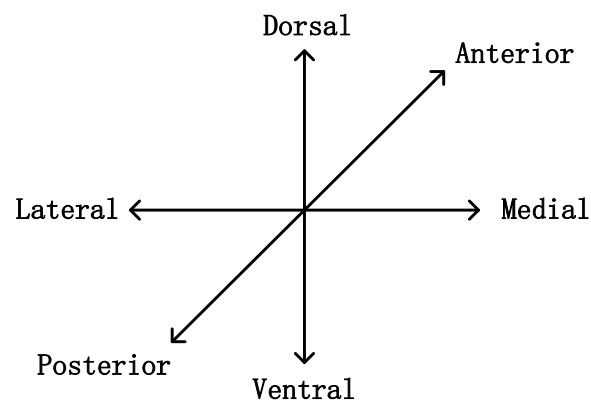
Figure 1.6 Anatomical Directions [7]

With respect to the determined trajectory, the microelectrode probes are slowly inserted into the brain in a stepwise manner. Usually, it starts recording about 8 to 10mm above the dorsal border of the target nucleus till 4mm below the ventral border of it. The recordings start and end at the same time for all five probes. And the recording duration for each location is normally about 10 or 20s. The sampling rate of MER signal is typically 12 or 24 kHz. After each recording, the MER needle will go 0.5mm deeper into the brain and start new recording.

Three MERs shown in Figure 1.7 were obtained at different locations inside the brain from the central probe. It can be seen that signal characteristics of these recordings, such as the signal amplitude and the background noise level changed a lot for different locations. Therefore, it is possible for the experienced neurologists to distinguish the recordings from different nuclei through both visually and audibly looking into the MER signals, and then make annotations of the target nucleus during the surgery.
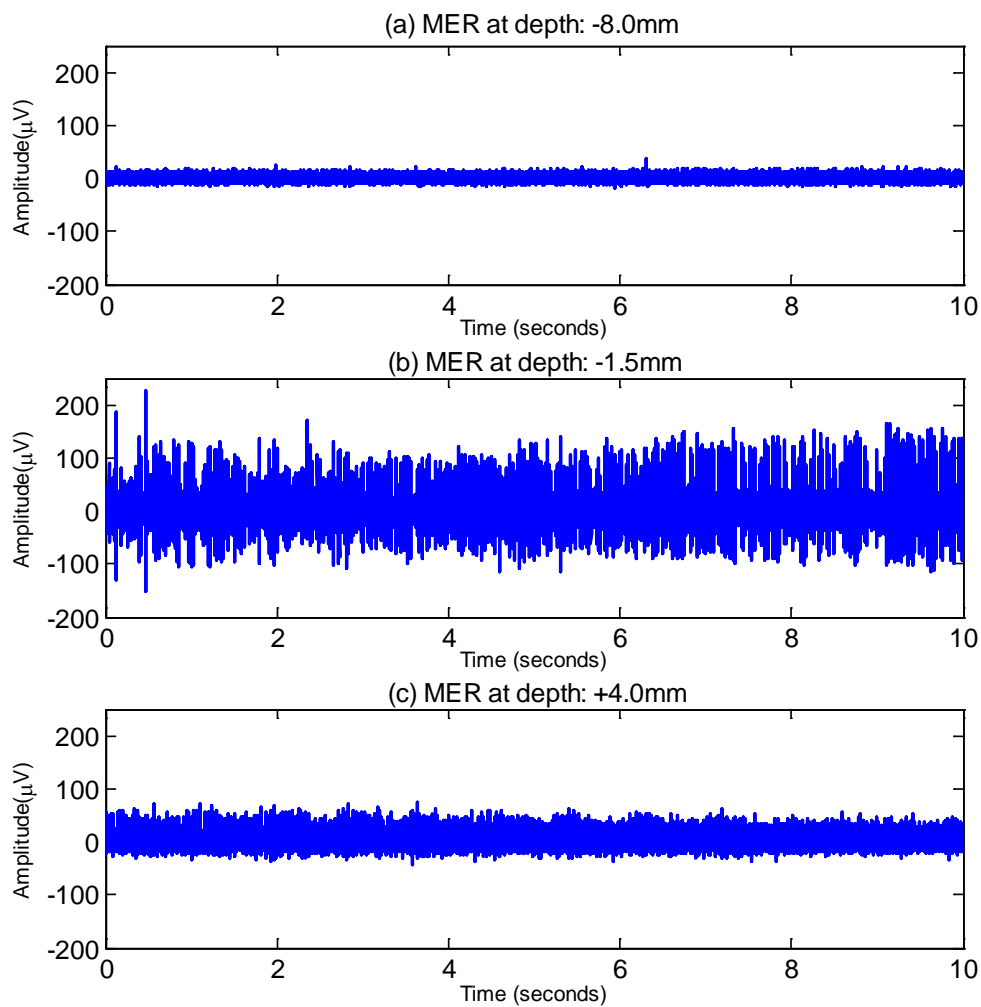
Figure 1.7 MER signal from different locations. Here shows three traces of MER signals recorded from three traces at different locations in the brain. The characteristics of the signal altered with respect to different location information.

1.4 Thesis Objective

The MER assessment requires a lot of neurologists' experience, so it is subjective and time consuming. Due to this, it is necessary to develop a supportive tool for assisting neurologists to process and analyze the MER signals.

The objective of the current work is to develop an algorithm for automated localization of STN from MER and also validate the algorithm by comparison to clinical ground truth data.

According to the objective, my thesis work is to first perform MER signal processing and analyzing and then develop an automated target nucleus localization algorithm for DBS electrode implantation. The target nuclei are STN and SN. STN is the target nucleus for implanting DBS electrode. And the reason for also locating SN is that it is very close to the ventral border of STN, so targeting it can increase our accuracy level of targeting the ventral border of STN.

1.5 Data Collection

A total of 84 data sets used for this study were obtained during DBS surgery at Academic Medical Centre hospital in Amsterdam, the Netherlands. The target nucleus for DBS surgery is STN. Each dataset contains MER signals recorded from all depths of five probes. 14 datasets were randomly chosen as training data sets to develop the targeting algorithm. And the rest 70 data sets were used to test the effectiveness of the resulting algorithm.
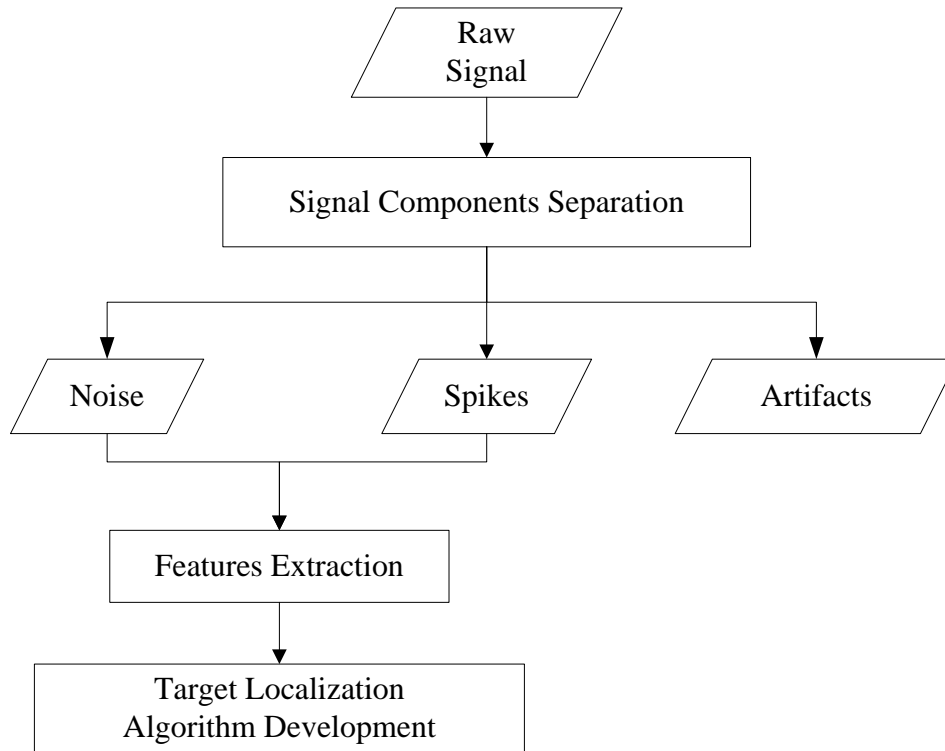
1.6 Thesis Work Flow

The structure of my thesis work can be divided into the following three tasks:
- Signal Components Separation
- Feture Extraction
- Target Localization Algorithm Development

The flow chart is illustrated in Figure 1.8:

Figure 1.8 Thesis work flow. The three tasks are: signal components separation, feature extraction and target localization algorithm development

The first crucial element of the work flow is to separte the 3 different signal components: noise, spikes and artifacts. The reason is that all of the signal characteristics for neurologists to distinguish the locations of STN or SN are depending on the changes of either background noise or spikes. Signal components separation is not an easy task because the MER signal we are dealing with is non-stationary, so the properties of it may vary from time to time. Besides, the background noise level is high and some of the artifacts look similar to real spikes thus cannot be easily distinguished from each other.

After that, with all three signal components separated, the next step is feature extraction. Based on the signal characteristics of the target nucleus, multiple computational features are extracted from the 14 training datasets. The purpose of this step is to find out the good indicators that show distinct characteristics for the target locations. The results of all features are compared with the neurologists' annotation afterwards and the best indicators are then integrated for the final step of developing the STN and SN localization algorithm.

# Chapter 2 Signal Components Separation

2.1 MER Signal Composition

The raw MER signals consists of three distinct components: background noise, action potentials and artifacts.[8] One recording of raw MER signal was shown in Figure 2.1.
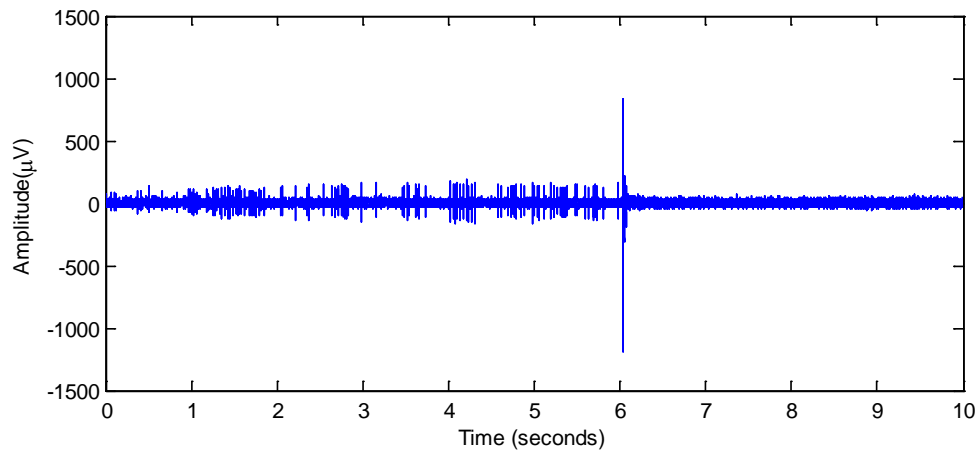
Figure 2.1 Raw MER signal. The raw MER signals is the combination of three distinct signal components: background noise, action potential and artifact.

The background noise is essentially the broad-band white Gaussian noise generated by the background neuronal activities, the electrical interference and other noise; Typically, the amplitude for background noise is from 2 to 6µV.

The action potentials, or say the spikes, are the neuronal activities recorded from nearby one or more neurons in a local region. Specifically one spike is composed of a positive part and a negative part as shown in the Figure 2.2. The average total duration for one spike is about 1-2ms. The time interval between the positive peak and the negative peak is around 0.5ms. The average peak amplitude is about 70µV, and normally it will not exceed 150µV.
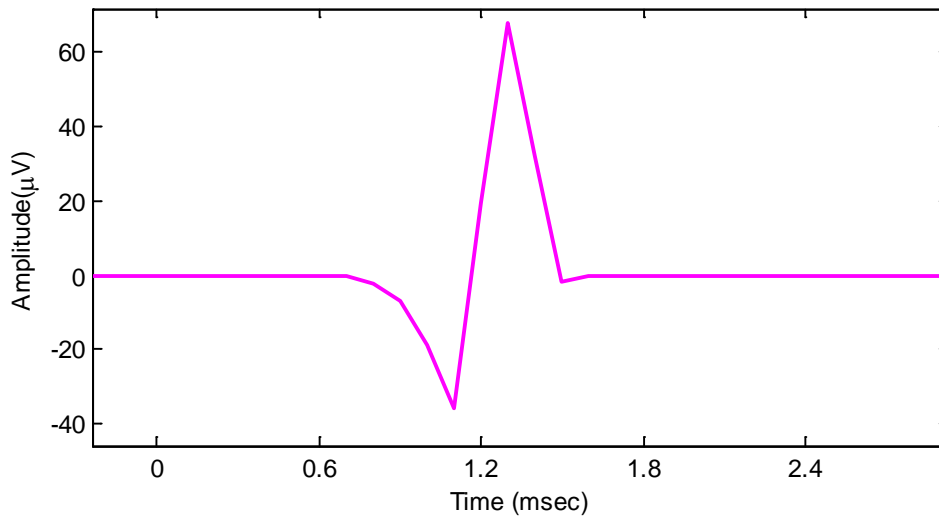
Figure 2.2 Spike. One typical spike has total duration approximately 1ms and positive to negative peak interval 0.5ms.

As to the artifacts, they may either result from the mechanical oscillations of the sterotactic frame that attached to the patient's skull or due to patient's speaking during the surgery. Typical artifact signal is oscillatory and compared with the background noise and action potentials, the amplitude of the artifact is extremely high (Figure 2.3).
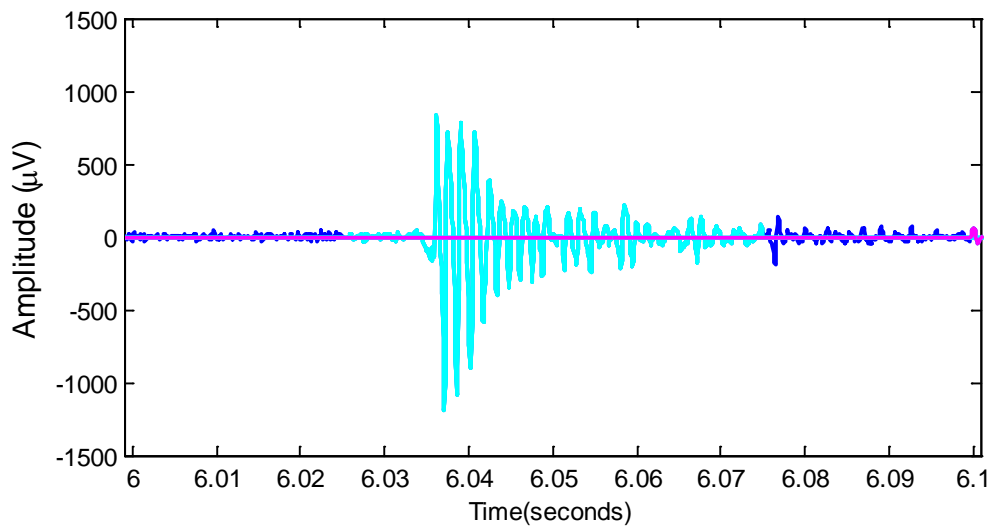
Figure 2.3 Artifact. One typical artifact has extremely high amplitude and compared with background noise and spikes. Oscilation is another characteristic of it.

2.2 MER Signal Components Separation Procedure

Three crucial elements for signal component separation were respectively noise level estimation, artifact rejection and spike detection. The Noise level estimation was applied first to the MER signal. The following steps of artifact rejection and spike detection algorithm were both determined relative to the estimated noise level.
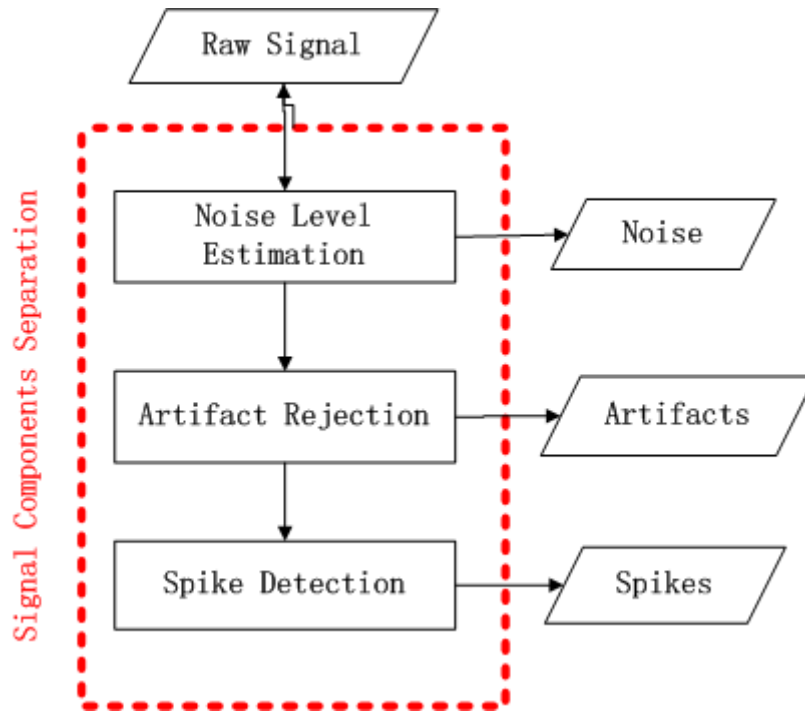
Figure 2.4 Procedure of signal components separation. Three steps for signal components separation are: noise level estimation, artifact rejection and spike detection.

2.2.1 Noise Level Estimation

The first step of signal components separation was to estimate the noise level bcause the background noise level tended to be stable during one single recording. We have tried three methods for noise level estimation: rms method, median method and noisemode method.

2.2.1.1 The Rms method

The conventional way for noise level estimation is to compute the standard deviation (rms) of the overall raw signal[8]. However, the drawback of this rms method is significant. This method is quite sensitive to the high amplitude 'outliers', even if only a small portion of the signal is contaminated. So the estimated noise level would

be accurate only if the whole recording is composed of just background noise. However, for our case, the spikes and artifacts are present in the recordings quite frequently and their amplitudes were much higher than the background noise.

2.2.1.2 The Median method

A better way for noise level estimation is the median method[8]. For gaussian distributed signal, the median of the absolute value of the signal and its standard deviation are proportional. By first taking the median of the absolute value of the raw signal, and then divided by a constant factor, we can get the estimation of the noise level.

$$\sigma_N = \frac{median\{|X|\}}{0.6745} \qquad (2.1)$$

### 2.2.1.3 Comparison of the Rms method vs. the Median method

The comparison of the rms method and the median method for noise level estimation was shown in Figure 2.5. The simulated signal was white gaussian noise (standard deviation equal to 1) added with artificial spikes. Each artificial spike had cosine shape with peak amplitude equal to 6 and total duration 2ms. It can be seen from the figure that with the increase of spike number in one recording, the estimated noise using rms method started to deviate from actual noise level very fast. The estimated noise calculated from median method performed much better. The deviation to the actual noise level was very small with less than 50 spikes. So if only a small portion of one recording contains spikes or artifacts, even if it has much higher amplitude than background noise, the estimated noise level will be accurate. However, with more spikes in the recording, or say, a large portion of the signal is contaminated by those 'outliers', the estimated noise level is not accurate anymore and we need a more robust method for noise level estimation.
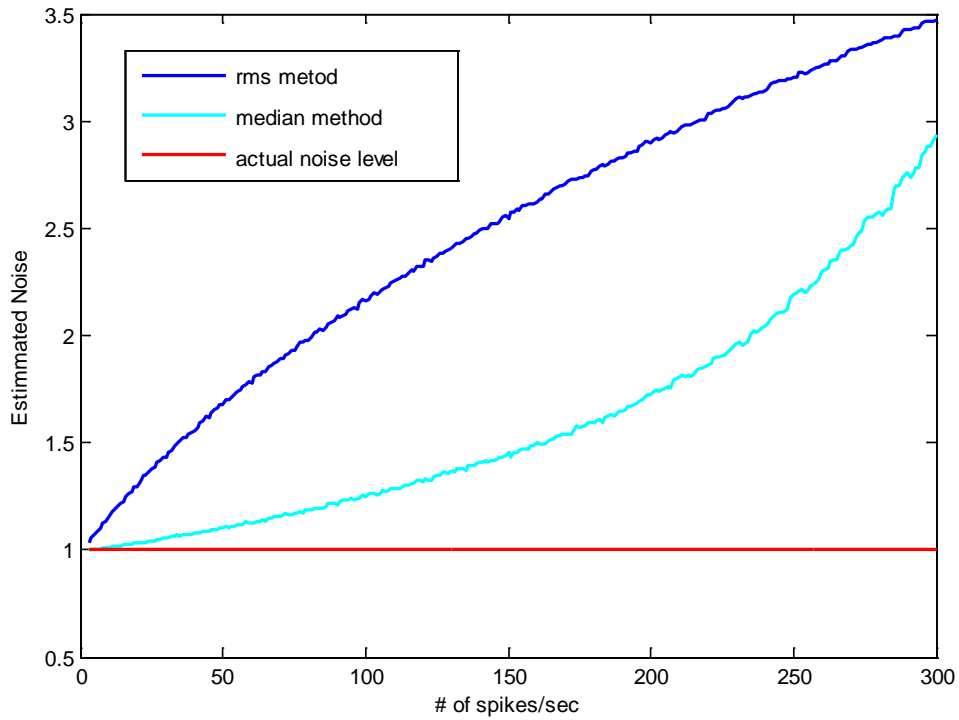
Figure 2.5 Noise level estimation. The bottom red line is the actual noise level which is equal to 1. The blue curve is the estimated noise level calculated from the rms method and the cyan curve is calculated from median method. With the increasing number of spikes, the estimated noise level from rms and median methods deviate from actual noise level with different deviation rate. When there are more artifacts and spikes present in the recording, the performances of the median method are always better than the rms method.

2.2.1.3 Noisemode method

For the case that a large portion of the signal were composed of spikes and artifacts, a much complicated but robust method for noise level estimation was the noisemode method[8]. Unlike the previous two methods, noisemode method is based on the envelope of MER signal but not the raw signal(Figure 2.6). Compared to the raw signal, the envelope signal has less fluctuation and therefore can better indicate the actual noise level.
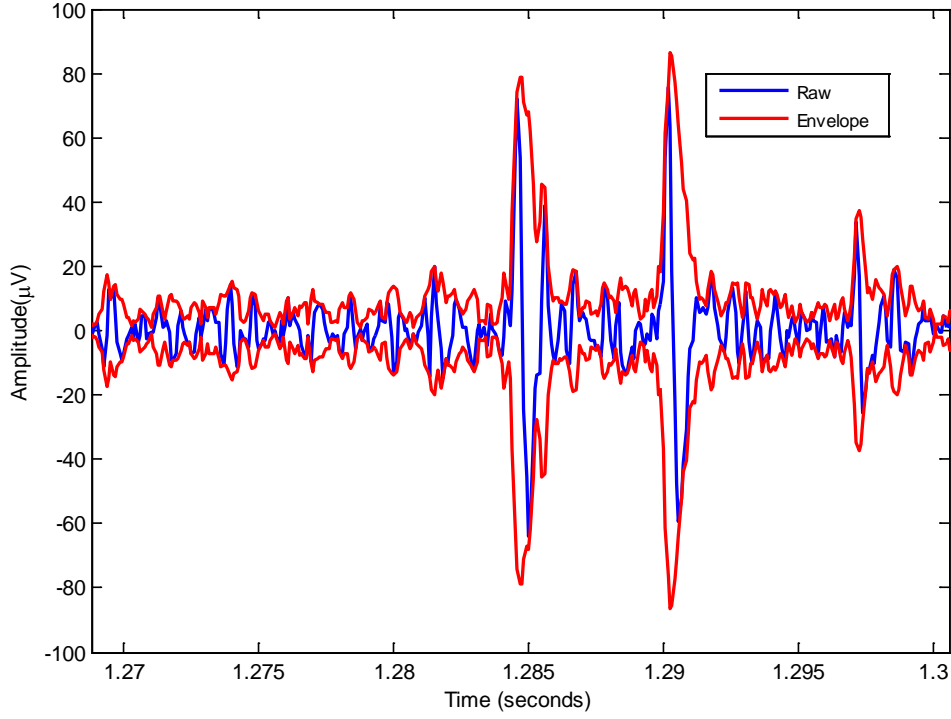
Figure 2.6 Envelope signal. The envelope of MER signal (red) was less fluctuating than raw MER signal (blue).

The computation of the envelope signal is done by first taking the Hilbert transform of the raw MER signal x(t). H(x(t)) is the Hilbert transformed signal.

$$H(x(t)) = \int_{-\infty}^{+\infty} \frac{x(t-\tau)}{\pi\tau} d\tau \qquad (2.2)$$

After that, a complex signal is constructed in the following way:

$$z(t) = x(t) + iH(x(t)) \qquad (2.3)$$

Z (t) is the envelope of raw MER signal. When the envelope signal obtained, the next step is to compute the amplitude distribution of the envelope (Figure 2.7). The reason that we turn to the amplitude distribution is that the amplitude ranges for spikes and artifacts are quite different from the background noise. Therefore, by limiting our histogram to cover only the range of data that is relevant to the background noise, we

found it fits Rayleigh distribution. (Theoretically, the envelope signal of white Gaussian noise follows Rayleigh distribution.)

$$P(z) = \frac{z}{\sigma^2} \exp(\frac{-z^2}{2\sigma^2})$$ (2.4)

The mode of Rayleigh distribution is most robust to the outliers. So the corresponding amplitude value is estimated as the background noise level.
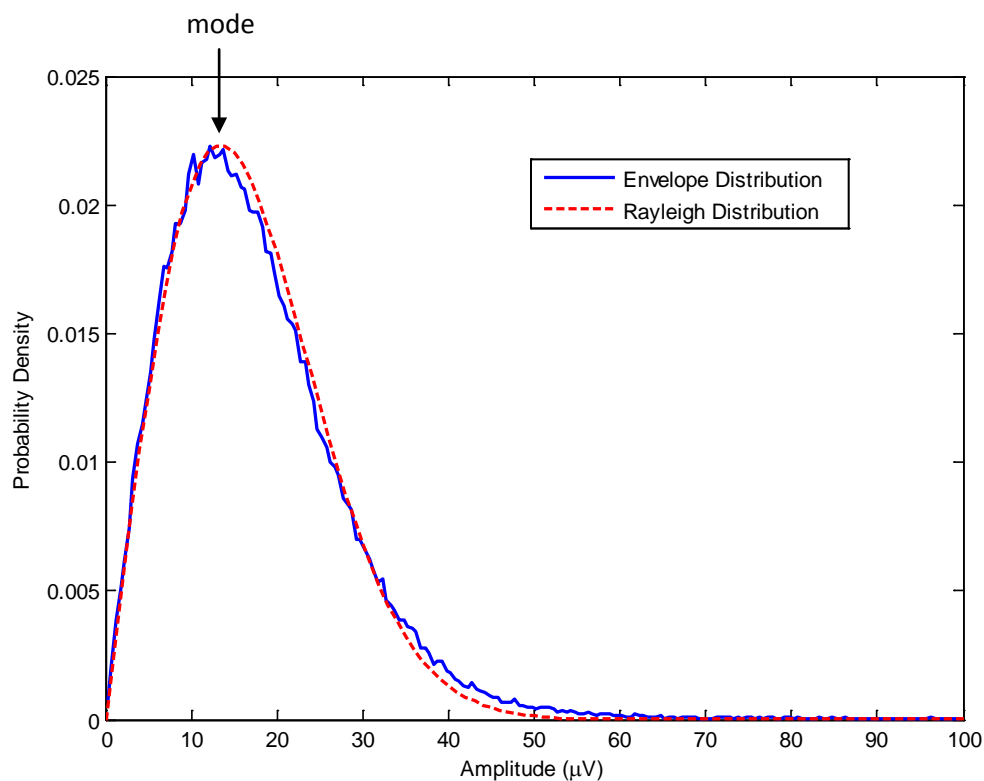

Figure 2.7 The envelope distribution. The distribution of the MER envelope is shown in blue and the red dashed curve is the standard Rayleigh distribution simulated in Matlab[9]. According to the plot, the envelope distribution closely follows a Rayleigh distribution.

2.2.2 Spikes & Artifacts Detection

After noise level estimation, artifact rejection and spike detection algorithm were applied to raw MER signal. Artifact rejection algorithm used an amplitude criterion relative to the estimated noise level. With all artifacts removed, the signal only contained the information of the background noise and spikes.

As to spike detection, we first set a threshold at 4 times the estimated noise level. For segments that exceeded this threshold, we then compared them with a spike template to check whether they were spikes or false positives. Figure 2.8 shows one example MER trace with all spikes and artifacts detected.
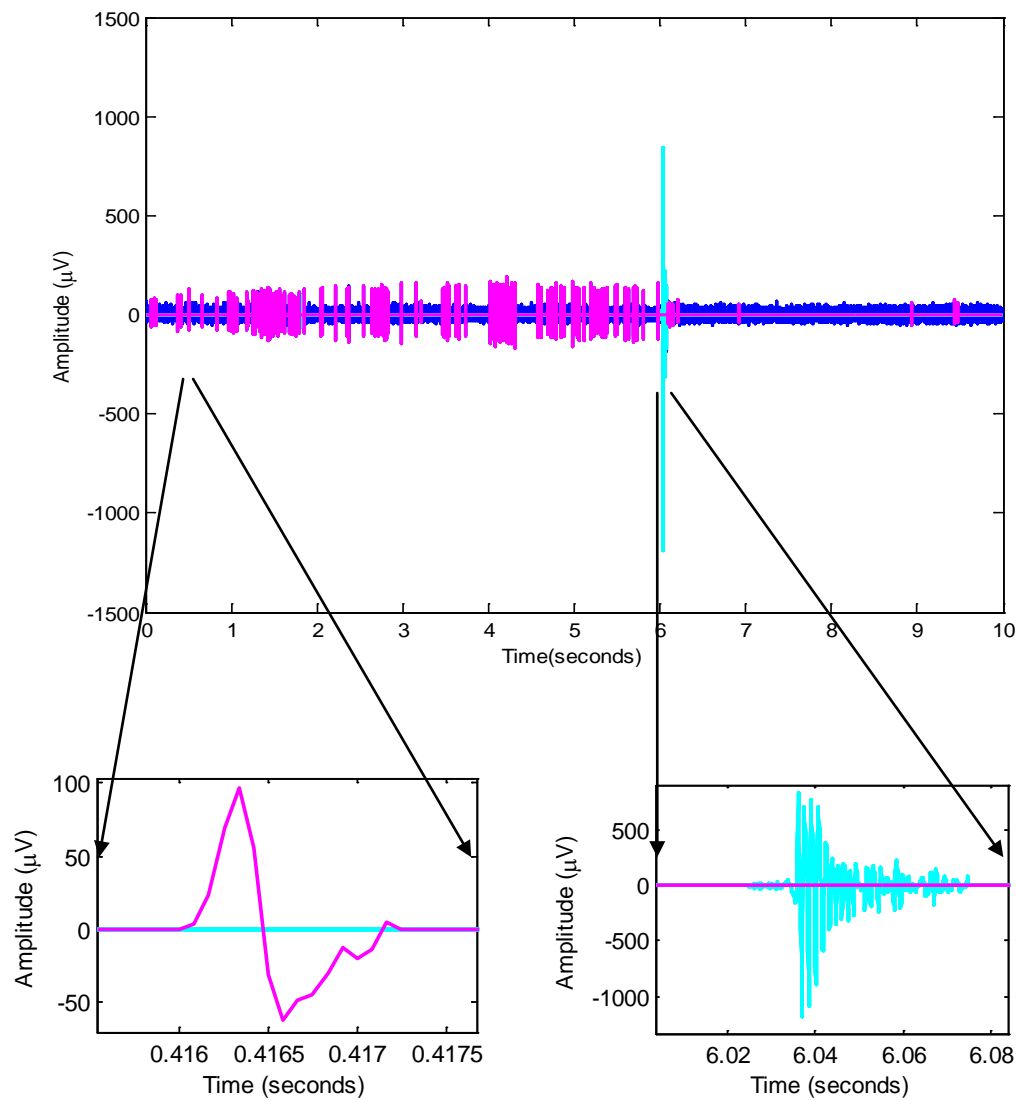
Figure 2.8 Spike and artifacts detection. In the upper figure, the background noise is shown in blue. Detected spikes were marked in pink and the rejected artifacts were marked in cyan. The lower two plots were one single spike and one typical vibration artifact.

Chapter 3 Feature Extraction

With all three signal components separated, the next step according to work flow was feature extraction[10]. 15 statistical measurements were calculated for each trace with each one extracted certain characteristic from the MER signals. The features' performances for ideal MER signals were analyzed at first. All features were then applied to the 14 training datasets and compared with the clinicians' annotation.

3.1 Signal Characteristics of STN & SN

Feature extraction was based on the characteristics of the target nuclei STN and SN. According to neurologists' description, the signal characteristics of the target nucleus STN are[10]:

    a. An increase in the background noise;
    b. An increased density of neuronal discharge;
    c. An irregular high rate neuronal activity (bursting activity).

Because of the high neuron discharge rate occurring in STN region, the amplitude of background signal increases significantly.

As the microelectrode entered SN area, the high firing rates are observed as well. However, the characteristics of firing pattern are no more irregular bursting but periodic firing.

The characteristics of different firing patterns are introduced in section 3.6.

3.2 Signal Types for Feature Extraction

According to these signal characteristics, feature extraction was applied to three types of signals:

    a. artifact removed signal
    b. spikes
    c. Interspike Interval (ISI)

ISI is the time interval between each two consecutive spikes.

3.3 Feature Extraction Method

Feature extraction was applied in the following way. For each dataset, all recordings from one channel (central, lateral, medial, anterior and posterior) were processed with the increasing depth value. Each recording corresponded to a depth value. Feature extraction was then computed for all depths with one feature value obtained corresponded to one depth value as well. An example is shown in Figure 3.1.
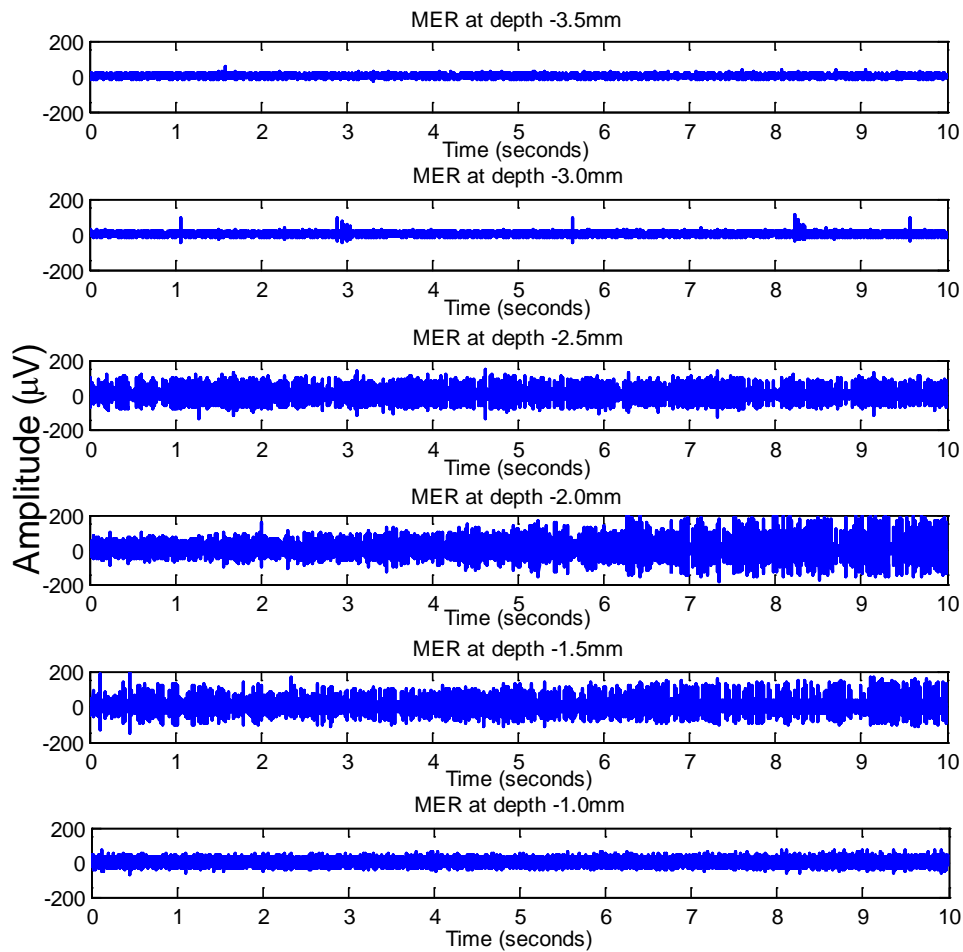
Figure 3.1 Illustration of feature extraction. Here shows MER signals with the increasing depth value (-3.5mm to -1.0mm). One feature value corresponded to one depth value.

The next step was to look into the trend of feature values' change with respect to the depth value (Figure 3.2).
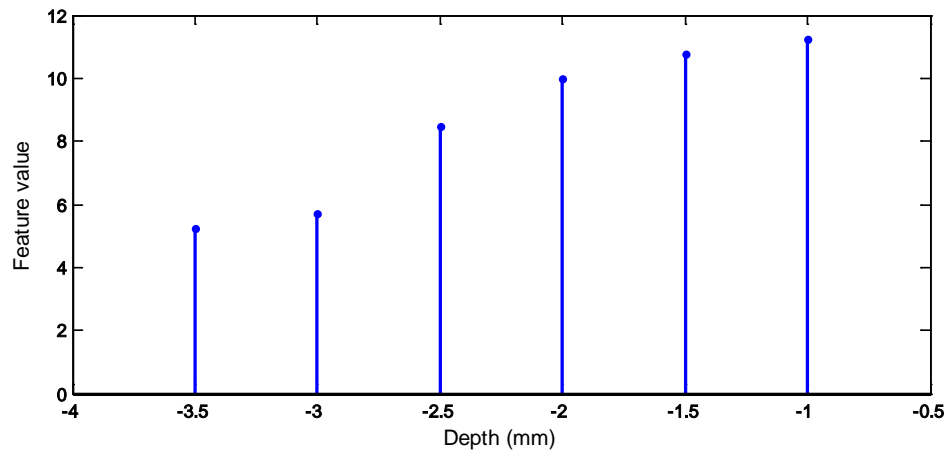

Figure 3.2 Illustration of feature extraction. Feature values were plot with respect to different depth value (location information).

3.4 Features Based on Artifact Removed Signal

Based on artifact removed signal, the features were calculated both in time domain and frequency domain. In time domain, the calculated features were: noisemode, curve length (CL), average nonlinear energy (ANE), and average absolute difference (AAD).

The way to calculate noisemode was the same as what we did for noise level estimation. The only difference was that the input signal was without artifact thereby reduced the fraction of outliers in the signal. Figure 3.3 is an example of feature noisemode extracted for all depths from certain channel of one patient. The result proved the high background noise level for the target nucleus STN. It showed that when the probe entering STN, noisemode increased significantly and stayed at high value until it exited STN. For the region between STN and SN, noisemode stayed at low level. But as soon as the probe entered SN, noisemode value increased again, however, comparing with noisemode value obtained within STN area, the noisemode for SN area had lower background noise level.
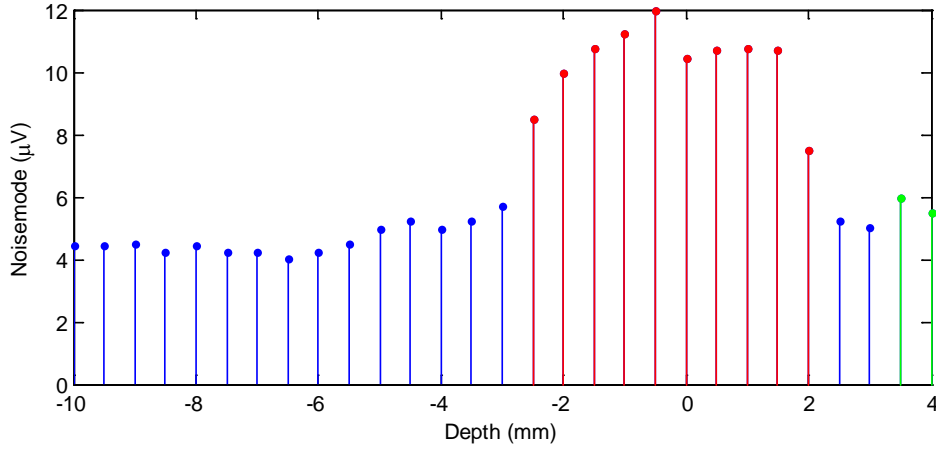
Figure 3.3 Noisemode. Depths in red and green were where clinicians annotated as STN and SN area. (This was the way we marked clinicians' annotation and it can be observed continually in the later figures.) The blue depths were the region outside of the target nucleus. It can be seen that Noisemode for STN and SN area were higher. The highest noisemode were obtained for STN area.

Curve Length (CL)[10] refers to the cumulative amplitude difference between two consecutive signal samples in one recording. So it measured how fluctuating the MER signal was. High CL value should be observed for high background activities.

$$CL = \sum_{i=1}^{N-1} | X_{i+1} - X_i |$$ (3.1)

X_i belongs to the artifact removed signal sample vector X={X_1, X_2, X_3... X_N}.

Figure 3.4 is the result of the CL measurement. Similarly to noisemode, CL increased when entered the target nuclei STN and SN.
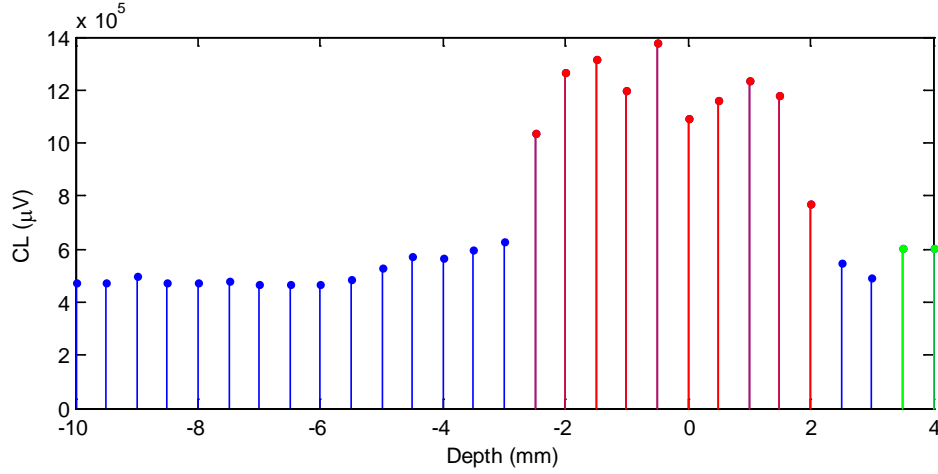
Figure 3.4 Curve length (CL). STN and SN have higher CL value due to the high background noise level.

Average Nonlinear Energy (ANE)[10] is the feature that measures the average energy difference between each signal sample and its two neighboring samples.

$$ANE = \frac{1}{N-2}\sum_{i=1}^{N-1} | X_i^2 - X_{i+1}X_{i-1} |$$ (3.2)

Again, X_i belongs to the artifact removed signal sample vector X={$X_1, X_2, X_{3...} X_N$}.

Average absolute difference (AAD) is the average amplitude deviation of each sample from the average amplitude of all samples. It measures the average signal deviation to the mean signal amplitude.

$$AAD = \frac{1}{N}\sum_{i=1}^{N} | X_i - \overline{X} |$$ (3.3)

X_i belongs to the artifact removed signal sample vector X={$X_1, X_2, X_{3...} X_N$}.

These two features are shown in Figure 3.5.
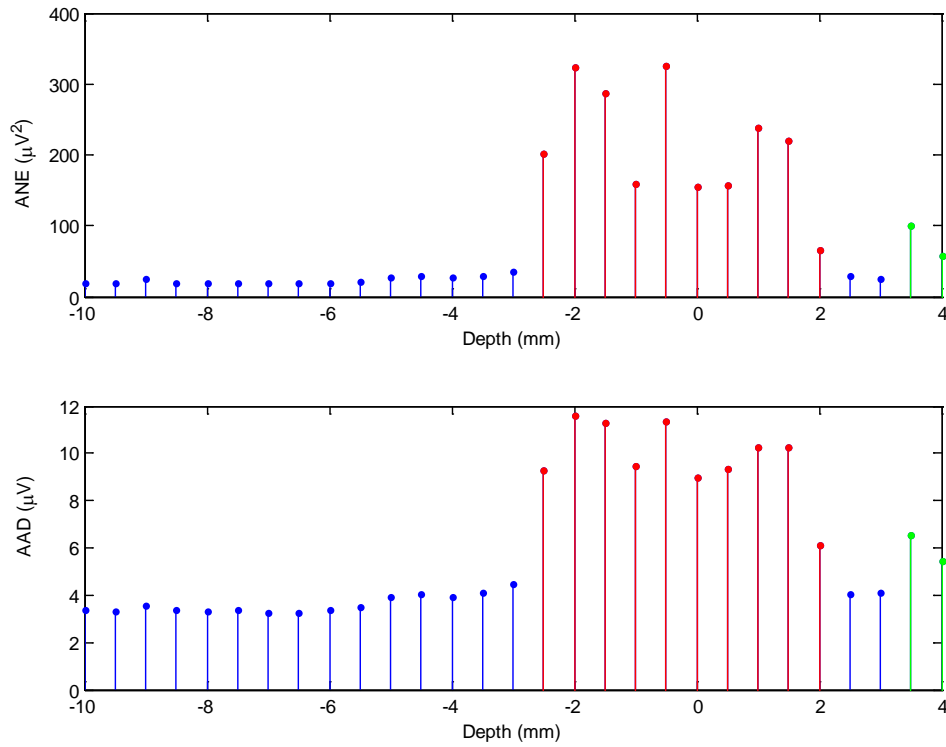
Figure 3.5 ANE and AAD. Depths in red and green were where clinicians annotated as STN and SN area. ANE and AAD have similar properties to curve length and therefore show similar results.

For the above three measurements (CL, ANE & AAD), if the whole trace mainly consists of background noise, moreover, the neuronal activities are contained in a small portion of the MER signal, these feature values would be close to zero.

Besides, several features were also calculated in frequency domain. The reason we turned to frequency domain was that synchronized oscillatory activity in certain frequency bands was one characteristic of STN[5]. The interested frequency bands were: low frequency band (1- 9Hz), alpha band (9-15Hz) and beta band (15-30Hz). Corresponded to these frequency bands, three individual frequency indices were calculated: low frequency index (LFI), alpha band index (ABI), and beta band index (BBI). To calculate these indices, power spectrum (PS) of the rectified signal were calculated at first by taking the autocorrelation of the signal and then Fourier transformed them into frequency domain. Rectified signal is the square of the artifact removed signal subtract the mean of the signal. This procedure shifts the power spectrum of the original signal to lower frequencies and enhances the peaks of firing.

Besides, an additional oscillatory index[5] (OI) was calculated. The forulars for these frequency indices are shown in Table 3.1. he frequency resolution for the power

spectrum was 1Hz/bin. The power spectrum of the first bin (0Hz) was excluded because it contains DC component that might lead to a high index value without real high neuronal activities happened.

| LFI	$LFI = \dfrac{PS(1-9Hz)}{PS(1-150Hz)}$	(3.4a)
BBI	$ABI = \dfrac{PS(9-15Hz)}{PS(1-150Hz)}$	(3.4b)
ABI	$BBI = \dfrac{PS(15-30Hz)}{PS(1-150Hz)}$	(3.4c)
OI	$OI = \dfrac{PS(1-30Hz)}{PS(1-150Hz)}$	(3.4d)

Table 3-1 Frequency Indices

Figure 3.6 and Figure 3.7 were two examples of frequency indices for two patients. Because of the inconsistence performance of these features, they were not chosen as final indicators for target nucleus localization.
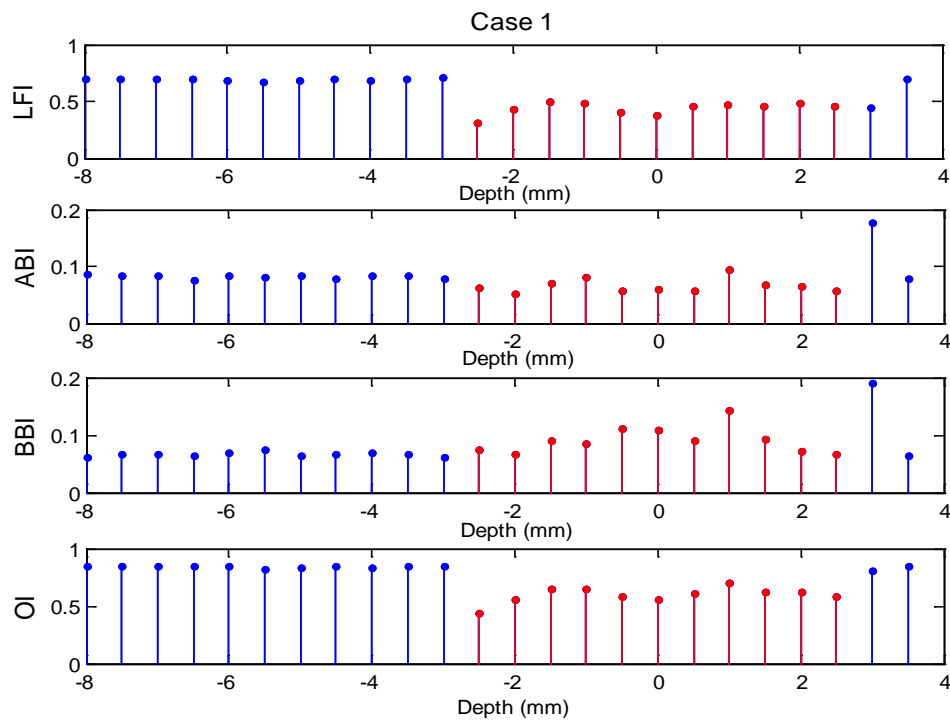
Figure 3.6 Frequency indices. For patient a (Case 1), LFI and OI decreased for STN area and there was no SN annotated.
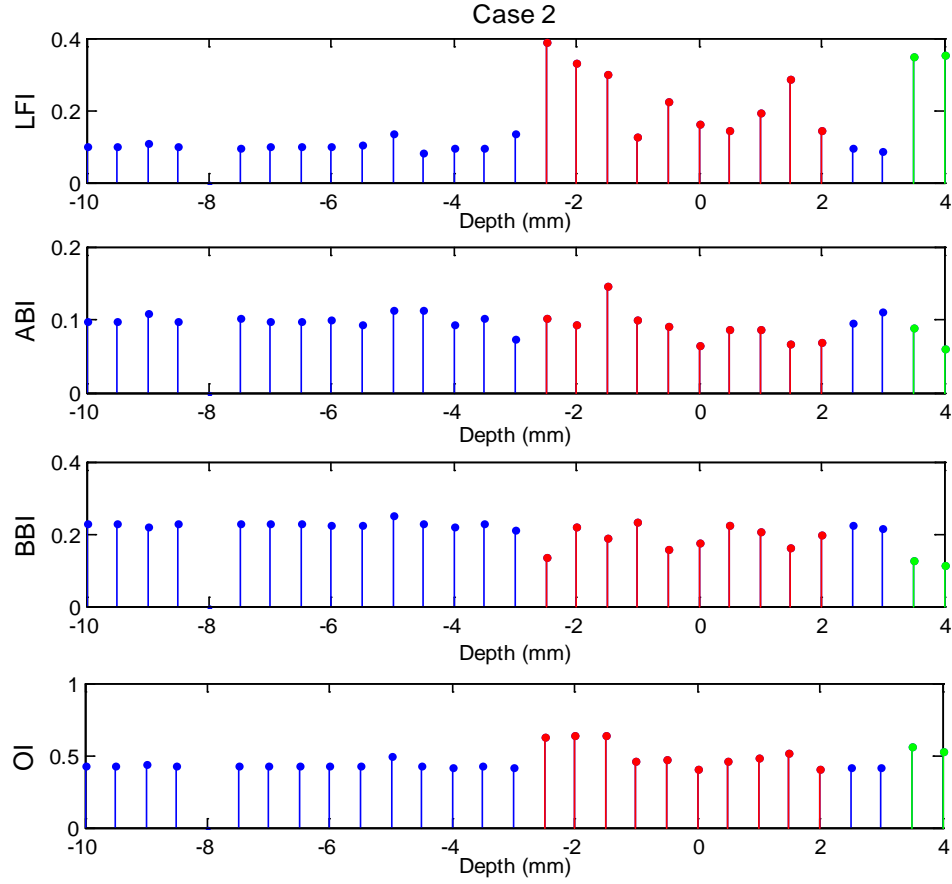
Figure 3.7 Frequency indices. For patient b, LFI and OI obtained higher value for STN area. However, the trends of the rest two features ABI and BBI for the target area were not clear.

3.5 Features Based on Spikes

Based on spikes, we computed the compound firing rate, which was the number of spikes in one second. According to the Figure 3.8, high firing rates were observed for STN & SN area. It should be noticed due to the fact that MER signals also contained neuronal activities from nearby multiple units, the measured firing rate was actually the "compound firing rate" if no spike sorting algorithm applied beforehand.
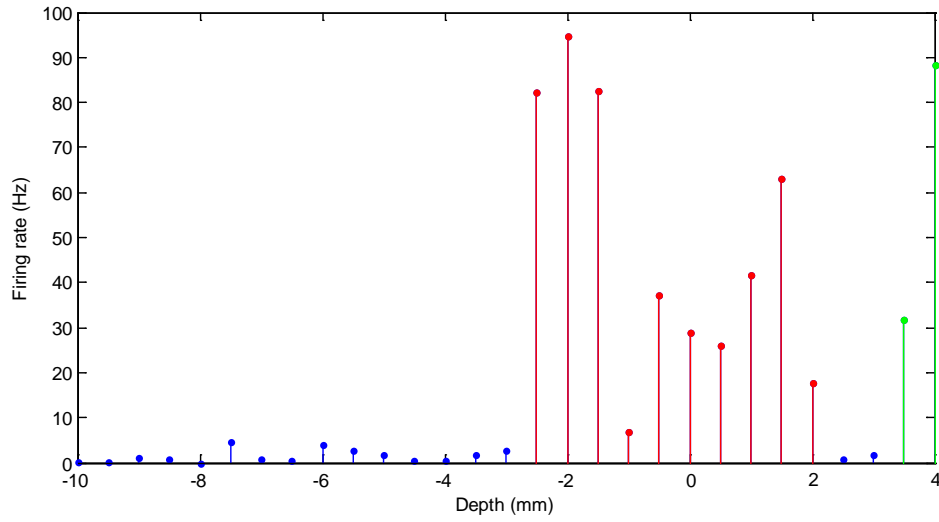
Figure 3.8 Firing rate. The compound firing rates obtained within STN and SN area were much higher than other regions.

3.6 Features Based on Interspike Intervals

In order to distinguish different firing patterns, feature extraction was applied with respect to inter spike interval (ISI). There are three firing patterns: tonic, random and bursting. Tonic means the neuron fires periodically. Random means ISI follows a Poisson process. Bursting is similar to tonic firing, but for each period, firing is repeated. Three firing patterns are shown in Figure 3.9.
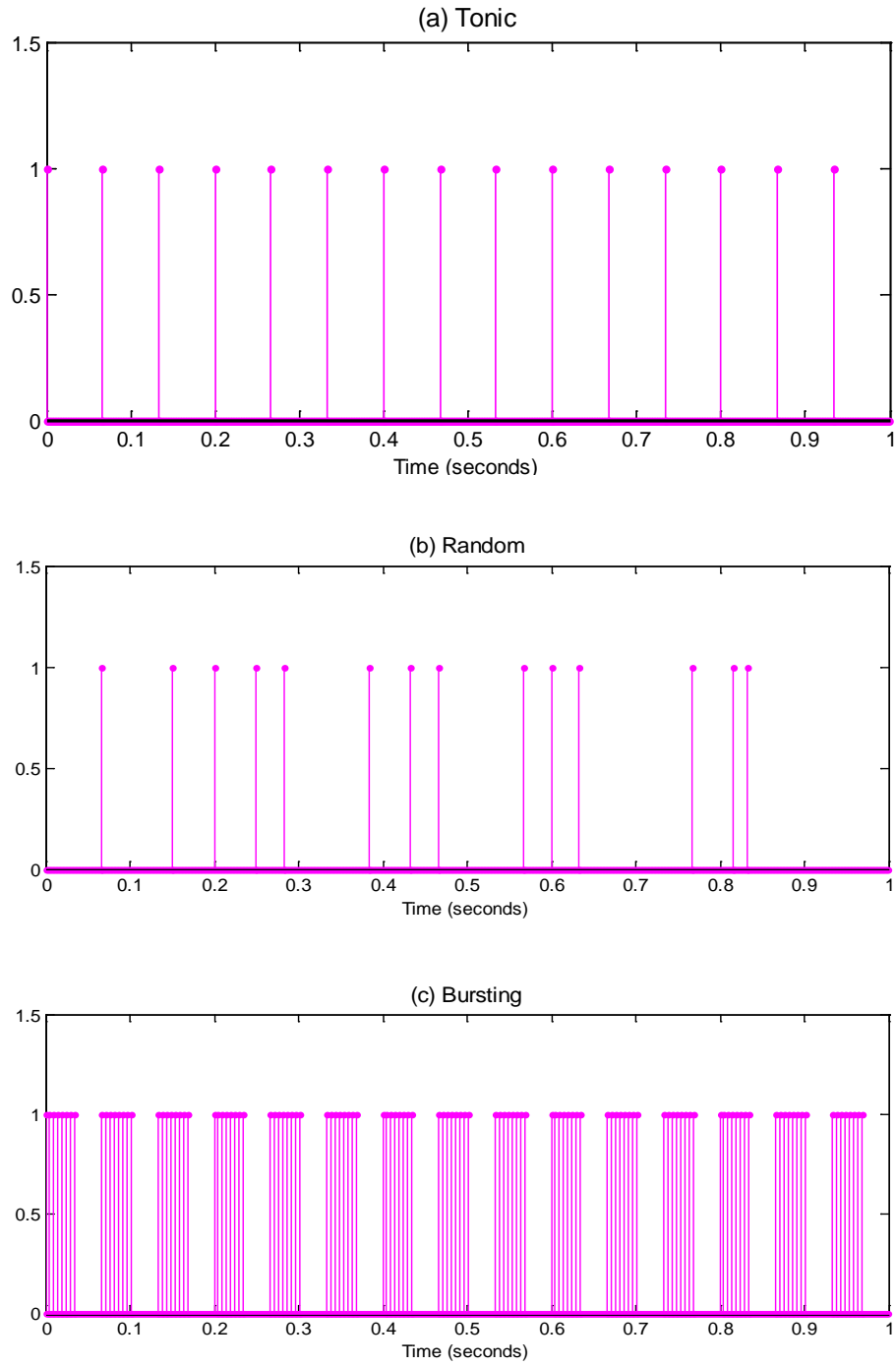
Figure 3.9 Firing patterns. Each pink delta impulse represented one spike in all of above figures. Tonic firing means neuron fires periodically. Random firing follows Poisson process. And the characteristics of bursting are periodicity and repeatability.

Based on firing patterns, the calculated features were: the standard deviation of ISI (ISI rms), modified burst index (MBI), pause index (PI), pause ratio (PR), poisson

surprise (PS), tonic index (TI), and the entropy of ISI distribution. Formula 3.5a-d is the calculation for ISI rms, MBI, PI, PR and TI.

$$MBI = \frac{\#(ISI < 10ms)}{\#(ISI > 10ms)} \qquad (3.5a)$$

$$PI = \frac{\#(ISI > 50ms)}{\#(ISI < 50ms)} \qquad (3.5b)$$

$$PR = \frac{\sum(ISI > 50ms)}{\sum(ISI < 50ms)} \qquad (3.5c)$$

$$TI = \frac{\sum \min(pre\_interval, post\_interval)}{total\_length} \qquad (3.5d)$$

All features depended on ISI were computed first on the signal simulated in Matlab that has single firing pattern to see how it should behave in theory and then apply to all the training datasets. This was because for real MER trace, multiple units might fire simultaneously with different firing patterns. And the obtained MER signal was the superposition of all units.

If one depth had less than ten spikes, we considered it as 'missing data', and artificially set all feature values to zero.

Theoretically, tonic firing and bursting have smaller ISI rms compared to random firing. As shown in Figure 3.10(a), ISI rms for tonic firing stayed at zero no matter how firing rate changed. This was because the ISI for tonic firing was fixed. Due to the irregularity of neural activities, random firing always had the highest standard deviation of ISI. The performances of bursting were between tonic firing and random firing. For high firing rate, the values of ISI rms were all converge to 0. This trend had also been proved from the results of the training datasets. One example is shown in Figure 3.10(b). The target nuclei STN & SN have lower value than other region.
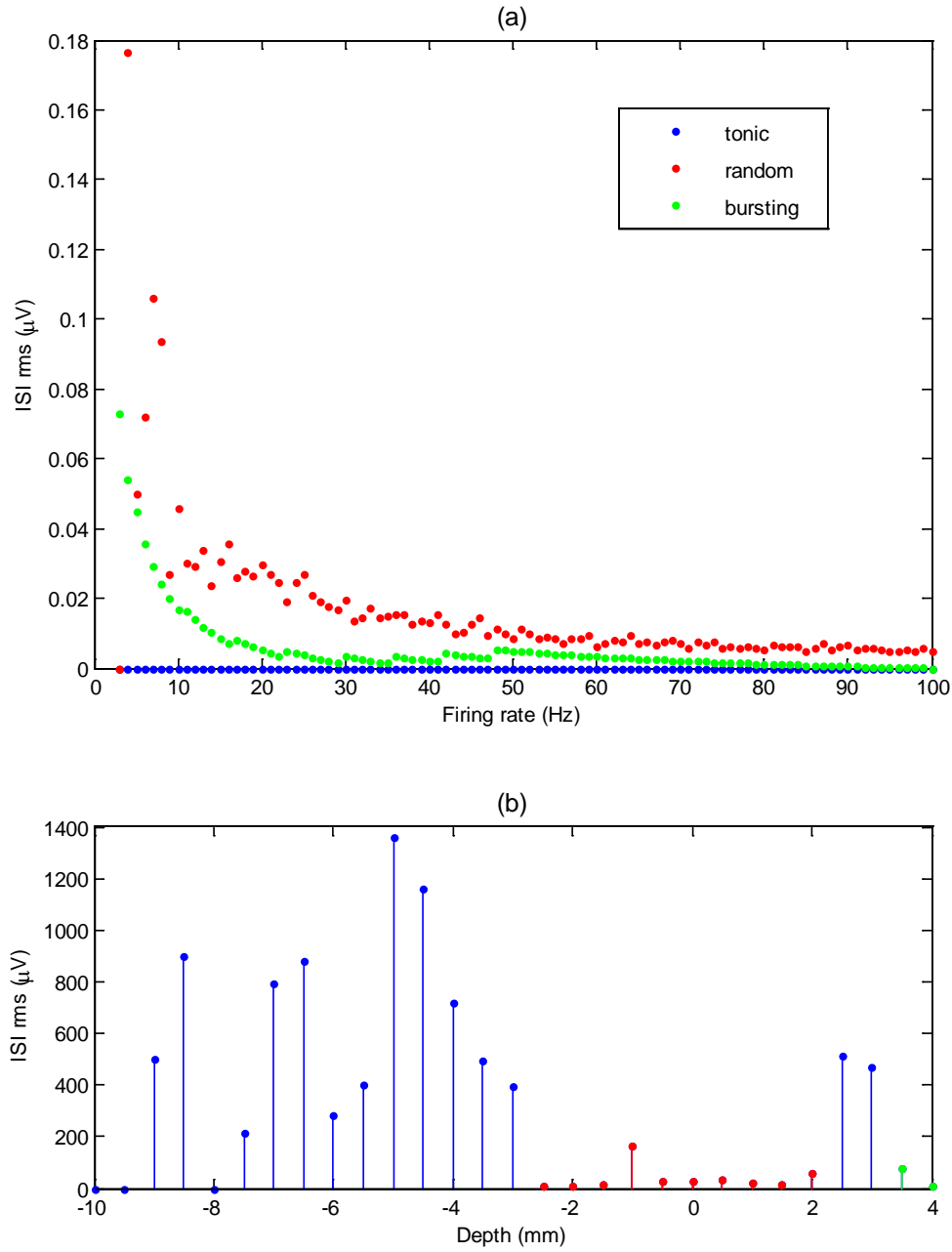
Figure 3.10 ISI rms. (a) Theoretically, with increasing firing rate, the ISI rms decreases for both random firing and bursting. Tonic firing had no ISI deviation because of its periodicity. (b) Particularly, for this training dataset, lower ISI rms had been observed for two target nuclei, which meant the neural activities for these regions were more regular. However, it can only distinguish between random and regular firing. For distinguishing tonic and bursting, ISI rms was not a good indicator.

MBI[10] is the ratio of the count of ISIs less than 10ms to the count of ISIs greater than 10ms. Bursting have more shorter inter-spike interval therefore should obtain high value as shown in Figure 3.11.
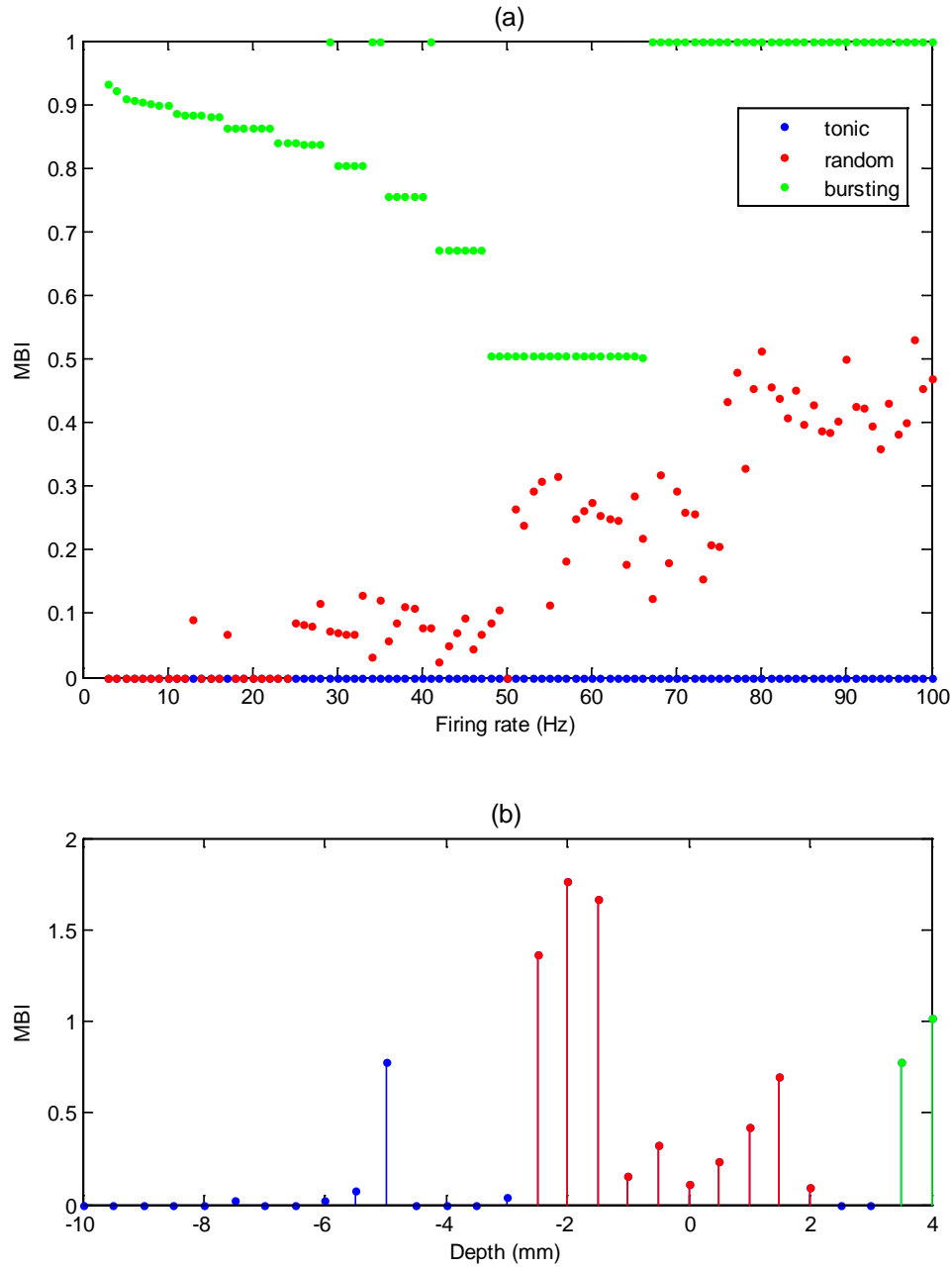
Figure 3.11 MBI. (a) Theoretically, when firing rate equaled to 100Hz for tonic firing, the length of ISI equaled to 10ms and therefore the MBI of it stayed at 0 all the time. MBI of random firing increased with increasing firing rate. As to bursting, the trend of MBI depended on how we constructed the firing pattern (such as the repeat time). (b) For one training dataset, it was observed that MBI values for the target nuclei STN & SN were higher when comparing with other regions.

PI[10] is the ratio of the count of ISIs that are greater than 50ms to the number less than 50ms; Similarly, PR[10] is the cumulative ISI time that greater than 50ms divided by the cumulative ISI time less than 50ms. Tonic and random firing have longer ISI so

higher value of PI and PR were observed both for the simulated signal (Figure 3.12) and the training datasets (Figure 3.13).
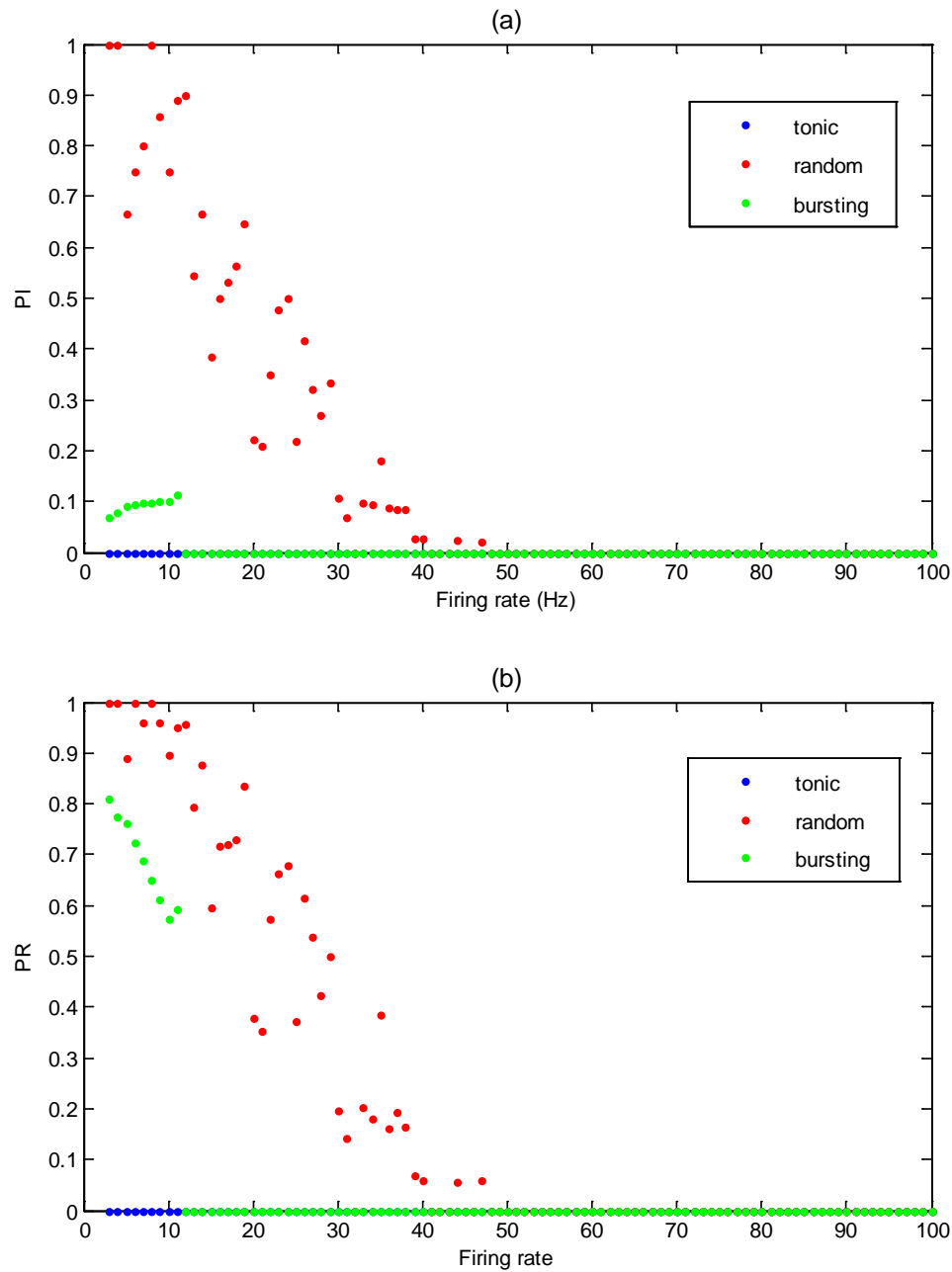

Figure 3.12 Theoretical PI & PR. PI and PR have similar characteristics. For high firing rate, the firing patterns converged to zero. As to low firing rate (less than 17Hz), random firing had the highest PI and PR. And for tonic firing, PR and PI always stayed at zero. The value of PR reduces according to the decreasing of ISI.
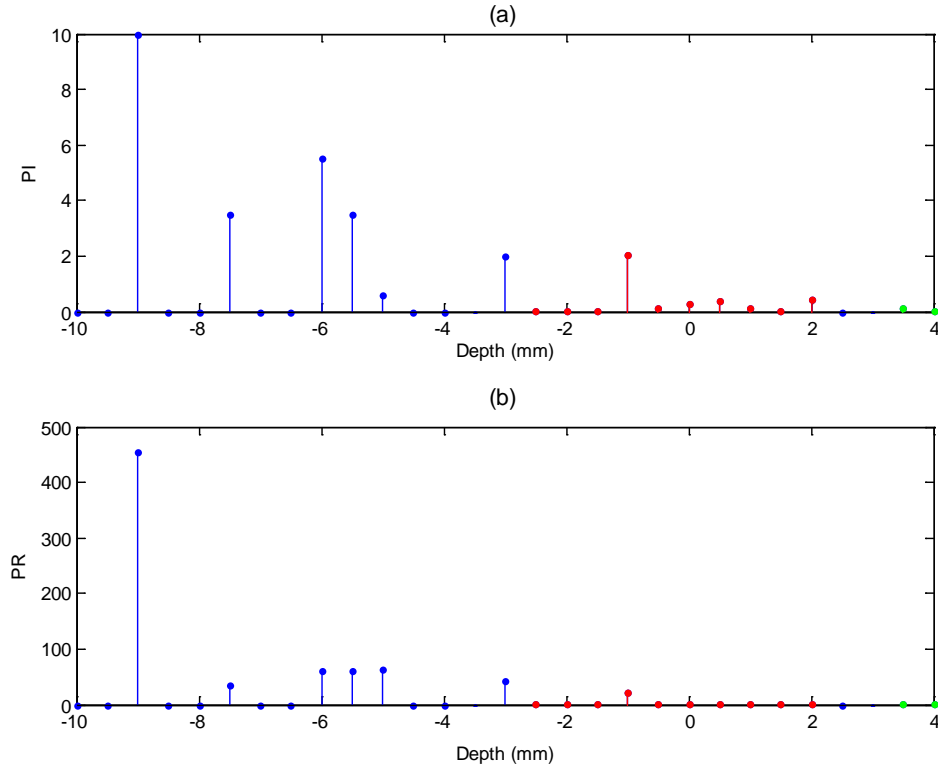
Figure 3.13 PI & PR for training dataset. Here is one typical result from the training dataset where low PR and PI value were observed for STN (bursting) & SN (tonic). However, for other regions (random), due to the non-stationary and multiple units firing, high values were not consistently obtained.

The shannon entropy[11] of ISI measures the randomness of the spike occurance. It was calculated in the following way: the distribution of ISI was calculated at first (Figure 3.14).
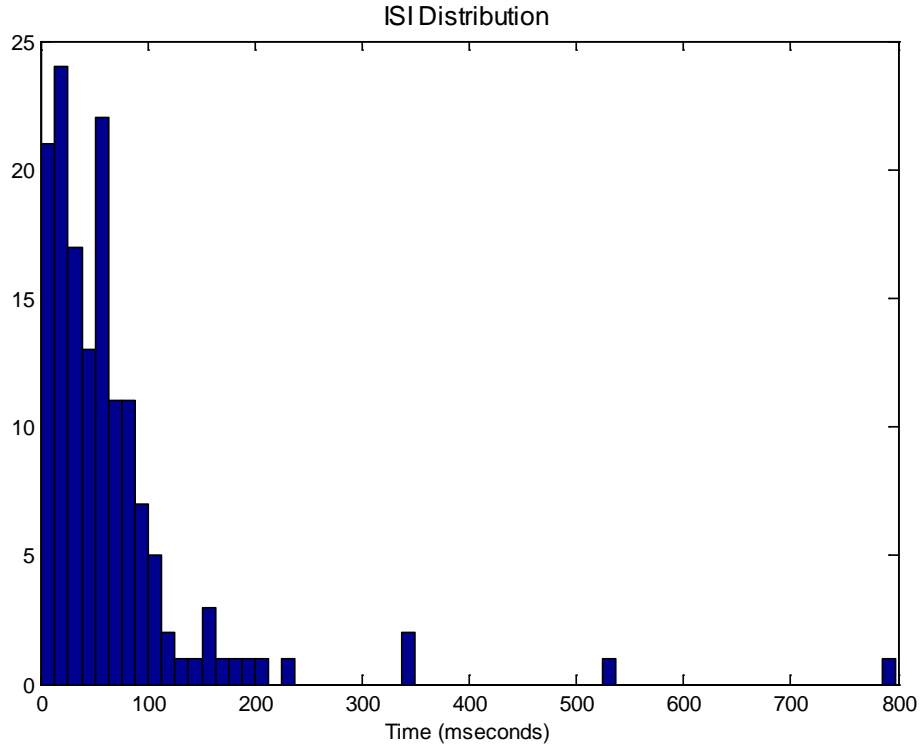
Figure 3.14 ISI distribution. The graph shows one example of the distribution of ISI. Only the bins not equal to zero were contribute to the calculation of the entropy.

None empty bins applied the formula 3.6 to get S_j:

$$S_j = - \sum_{None\_zero\_bins} freq\_bin(i) * \log(freq\_bin(i))$$

(3.6)

Smax was calculated afterward with known the decided number of bins as formula 3.7:

$$S_{max} = \log(\# bin)$$

(3.7)

Using S_j and S_{max}, the obtained Shannon Entropy was shown in formula 3.8:

$$Entropy = \frac{S_{max} - S_j}{S_{max}}$$

(3.8)

Lower entropy corresponded to random firing pattern. For the regular firing patterns (tonic and bursting), the entropy was high (Figure 3.15). The result for training

34

datasets shown in Figure 3.16a had good performance because of the different engropy ranges for target nuclei and other regions. But it shoud be noted that the depths outside the STN & SN were artificially set to zero. If we didn't consider firing rate as a constrain, then the result of the real entropy obtained (Figure 3.16b) was quite fluctuating and couldn't be used for distinguishing the target nuclei from other regions.
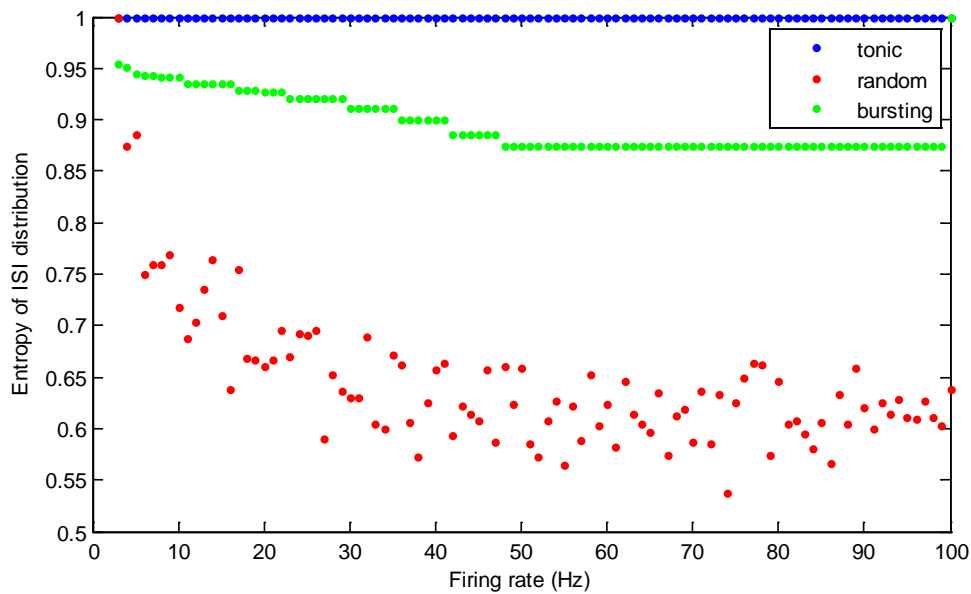

Figure 3.15 Theoretical entropy of ISI distribution. Because of regular neural activities of tonic firing and bursting, high entropy value should be obtained. On the opposite, the entropy values for random firing are quite low.
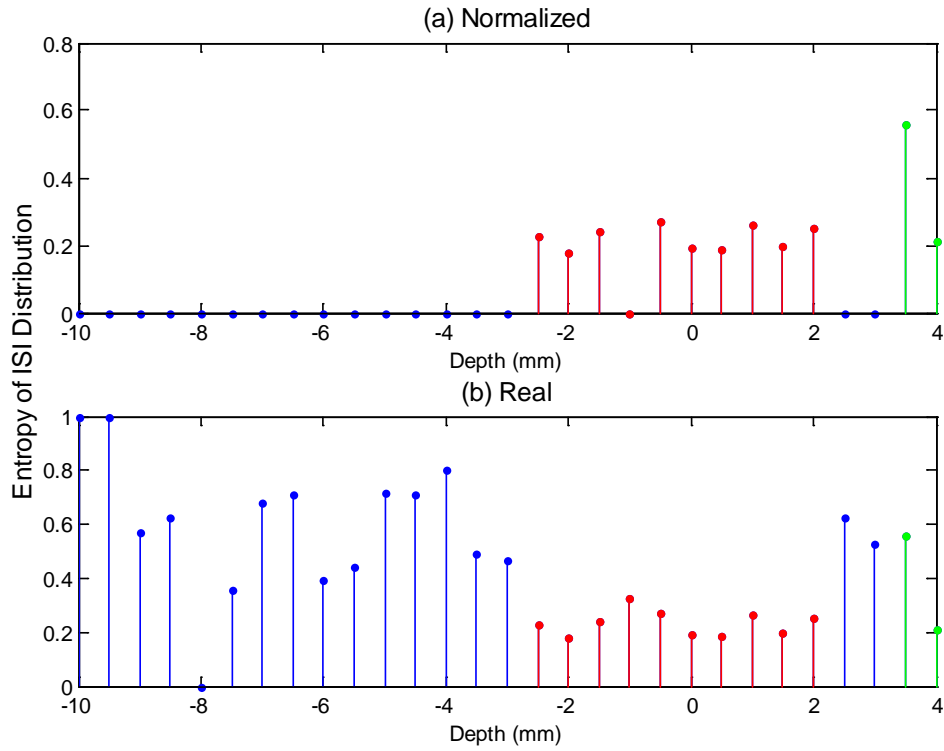
Figure 3.16 Normalized and real entropy of ISI distribution. The difference between the entropy calculated in (a) and (b) is that for (a), we artificially set the entropy value for depth with less than 100 spikes to zero. And if that constrain removed, the performance of entropy measurement was not satisfied as shown in (b).

TI was another feature based on ISI. For each spike in one recording, we peaked the shorter interval between previous ISI and the next ISI (Figure 3.17). TI is the ratio of the summation of all of these shorter ISIs to the summation for all ISIs.
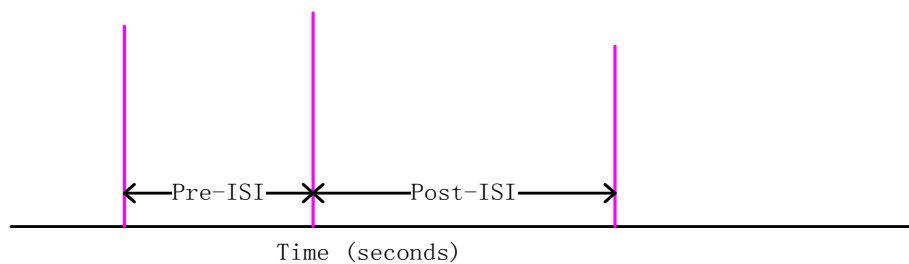
Figure 3.17 TI. Red stem represent spike. The pre-ISI and post-ISI weee compared for each spike. The one with shorter lengh was chosen. And TI is the summation of all these short ISIs divided by total length of all ISIs.

Ideally, if the recorded MER signal was tonic firing, this index should be approximately equal to 1 (Figure 3.18 (a)). However, due to the multiple units firing and the different firing patterns combination, no clear trend was shown in the trainning datasets (Figure 3.18 (b)).
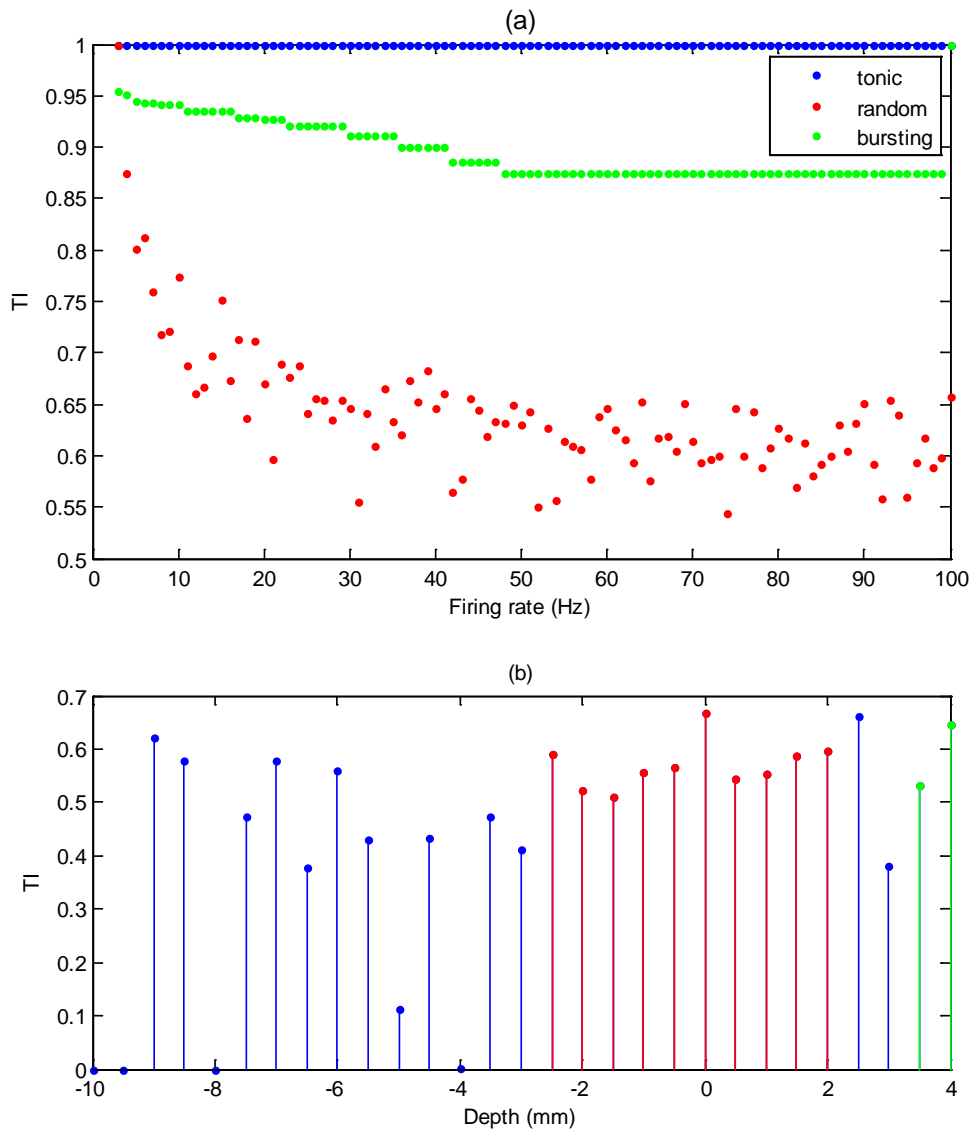
Figure 3.18 Theoretical and real TI. For generated signal, TI for tonic firing was always equal to 1. The trend of TI for bursting was stable at high value too (around 0.9). Comparing with tonic firing and bursting, TIs for random firing were relatively low. When applying on training datasets, the trend of TI was not clear at all for distinguishing STN & SN.

Neuronal signal processing was nonstationary, which meant the firing patterns of neuronal activity changed with time. In order to understand the changes of neuronal

37

activities, sliding window analysis was come in handy for extracting discernable information from different periods in one trace.

Within each of these windows, the stochastic nature of the neuronal signal could be considered as stationary signal and the nature of the neuronal activities could be seen as random firing with ISI Poisson distributed. Poisson Surprise (PS)[12] was used for evaluating the probability of the occurance of irregular events. Therefore, PS was introduced as one measurement for distinguishing bursting and tonic activity.

In the formula 3.9, n is the number of spikes contained in one window epoch (50ms), r is the averge firing rate computed in 1s interval that symmetrically around that 50ms window, and T is the time interval for the window size. Then, the probability P of the randomness within one window could be calculated by:

$$P = e^{-rT} \sum_{i=n}^{+\infty} \frac{(rT)^i}{i!} \qquad (3.9)$$

PS is given by equation 3.10:

$$PS = -\log(P) \qquad (3.10)$$

The upper plot in Figure 3.19 was one trace of MER signals obtained within the STN area, and the lower plot is the PS. The window size was set to 50ms. High PS was observed for the window with much higher firing rate compared to the average firing rate. Since the way we calculated PS involved windowing analysis, it could not represent the firing patterns with one single value. However, if no windowing analysis applied, the result of PS measurement would be similar to TI. Due to the non-stationary datasets and multiple units firing, this feature was not useful for target nucleus localization.
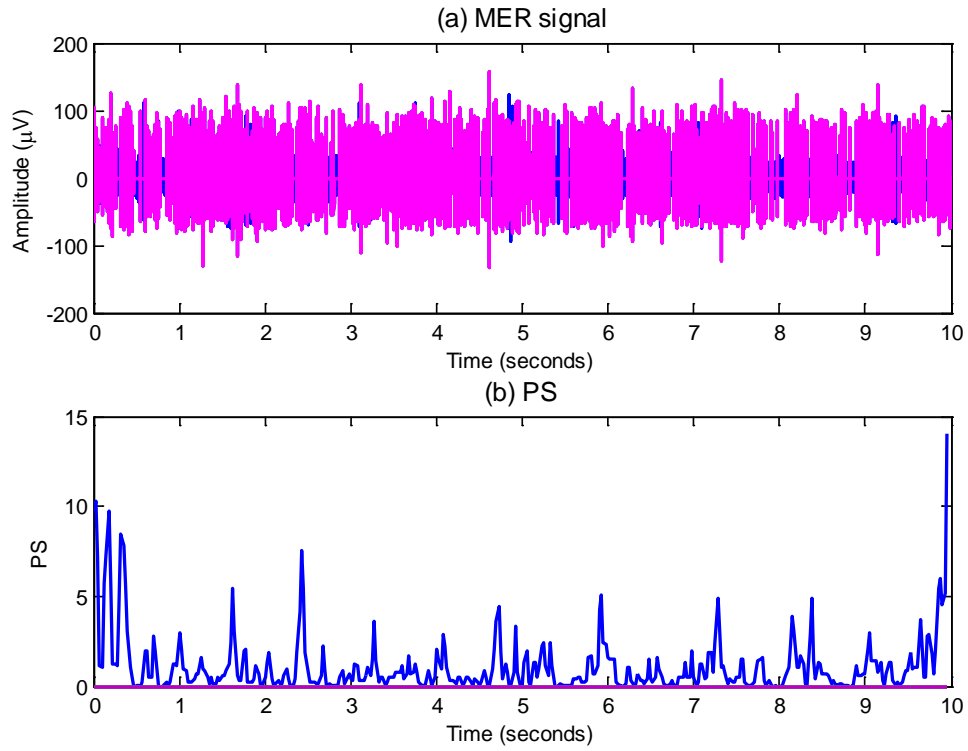
Figure 3.19 PS. (a) shows the MER signal for one depth and (b) is the resulting PS computed from every 50ms window of the MER signal. Dense neural activities leaded to high PS since more spikes obtained with comparison to the average firing rate. The high PS values in the first 0.5s and the last 0.5s were due to the transcending period.

Chapter 4 Resulting Target Localization Algorithm

14 datasets were randomly chosen as training datasets from 84 datasets that obtained from AMC hospital in Amsterdam. All of the above features were applied on these training datasets. After comparing them with clinical annotations, we found that any single measurement of neuronal activities was not reliable for target nucleus localization. Thus, the localization algorithm should be an integration of multiple measurements with each one carrying on certain independent information.

According to the observation of feature performance in Chapter 3, we found the noisemode that indicated the increasing background noise level and firing rate that indicated the increased neural discharge rate had consistent good performance and were therefore chosen for developing STN & SN targeting algorithm.

The features based on artifact removed signal(CL, ANE, AAD) had similar performance to noisemode but with more fluctuation thus less optimal for applying threshold detection. Due to the non-stationary datasets and multiple units firing simultaneously, the trends for frequency indices had no regularity and cannot used for assisting target localization.

For features depended on ISI, such as MBI, PI, PR, they showed certain characteristics for different firing patterns generated according to theory. But when applying to the real training datasets, it was hard for us to select baseline and applying threshold detection for target localization because of the intense fluctuation among the depths.

Besides, the performance of the entropy of the ISI distribution was mainly depended on the changes of firing rate. Without taking firing rate into account, the entropy of ISI for real MER signals obtained from 14 datasets provided no useful information for distinguishing different firing patterns. The performance of TI was similar to the entropy of ISI. PS can distinguish different firing pattern for one single MER trace, using windowing analysis. But when we averaged the performance for the whole trace, the result would be similar to TI and it was therefore not used for developing the target localization algorithm.

4.1 Target Nucleus STN Localization Algorithm

Specifically, the development of our targeting algorithm was as follows:

For STN targeting, we set thresholds for noisemode and firing rate respectively (Figure 4.1).
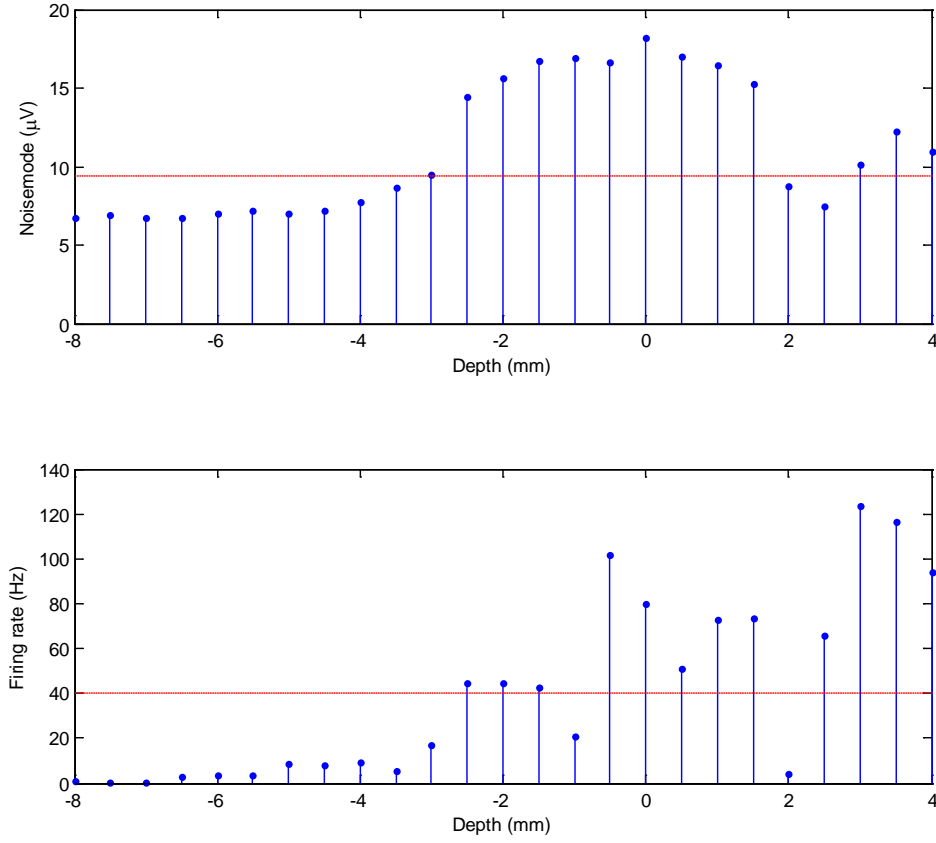
Figure 4.1 Threshold detection. Here shows one example from our training datasets. Noisemode and firing rate were calculated for all depths. The threshold detection was applied afterwards. The red dashed lines were the thresholds for noisemode and firing rate.

For noisemode, each time when noisemode exceeded this threshold, it should be marked as a candidate STN depth. However, how to optimally set this threshold was a difficult problem. It was impossible to find the perfect threshold, but the threshold should be chosen in a way that false positive and false negative are both minimized when comparing with clinical annotation. Based on the trainning datasets, the final thresholding for noisemode was set to the median of noisemode baseline multiplied with a constant factor(chosen as 1.35), and the first 10 depths were chosen as baseline. These two values were chosen so as to achieve the highest agreement level with clinicians' annotations.

Similarly, for the other good indicator compound firing rate, the threshold was set to the average firing rate over all depths.

41

After running through all 14 datasets, there were two cases confronted with respect to noisemode and firing rate thresholds. The first case was that some depths survived from the noisemode threshold and some depths exceeded the firing rate threshold as shown in Figure 4.2.

In order to annotate the dorsal border of STN, we first searched the first depth that exceeded both thresholds and marked it as depth 'x'. From that depth 'x', we searched backwards till the depth that the noisemode wnet below threshold. The last depth that above the noisemode threshold was marked as depth 'y'. Then, from that depth 'y-1', we checked its firing rate. If the firing rate was still above the threshold as shown Figure 4.2a, the algorithm would continually searching backwards and annotated the dorsal border of STN at depth before firing rate dropped below threshold. Otherwise, if the firing rate is already below threshold, we annotated the dorsal border of STN as shown in Figure 4.2b.
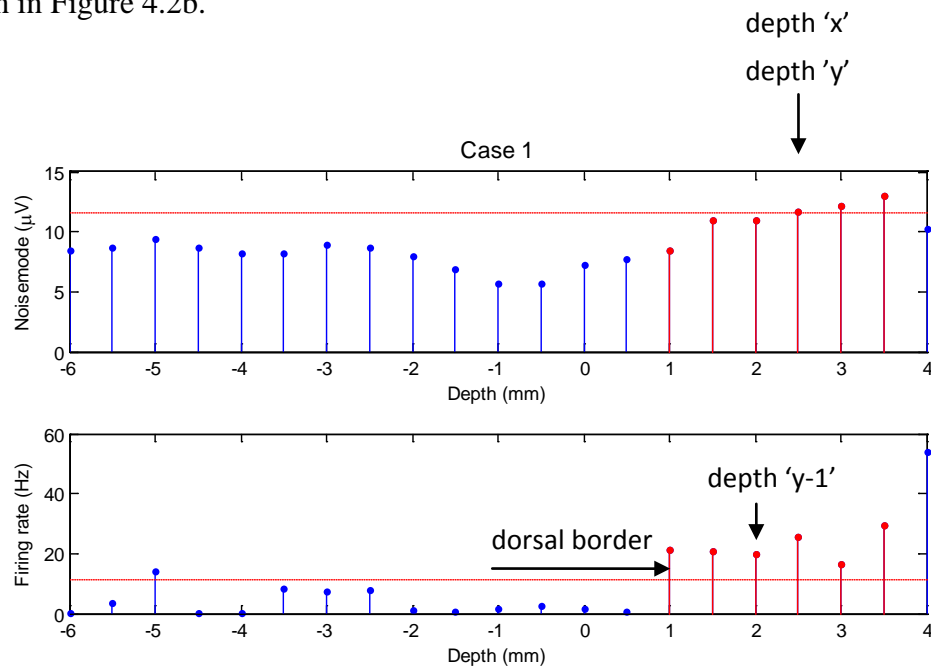

Figure 4.2a STN detection (dorsal border). For this case, depth 'x' and depth 'y' were both located at depth +2.5mm. Firing rate for depth 'y-1' was still above the threshold. The depths marked in red were the annotated STN area.
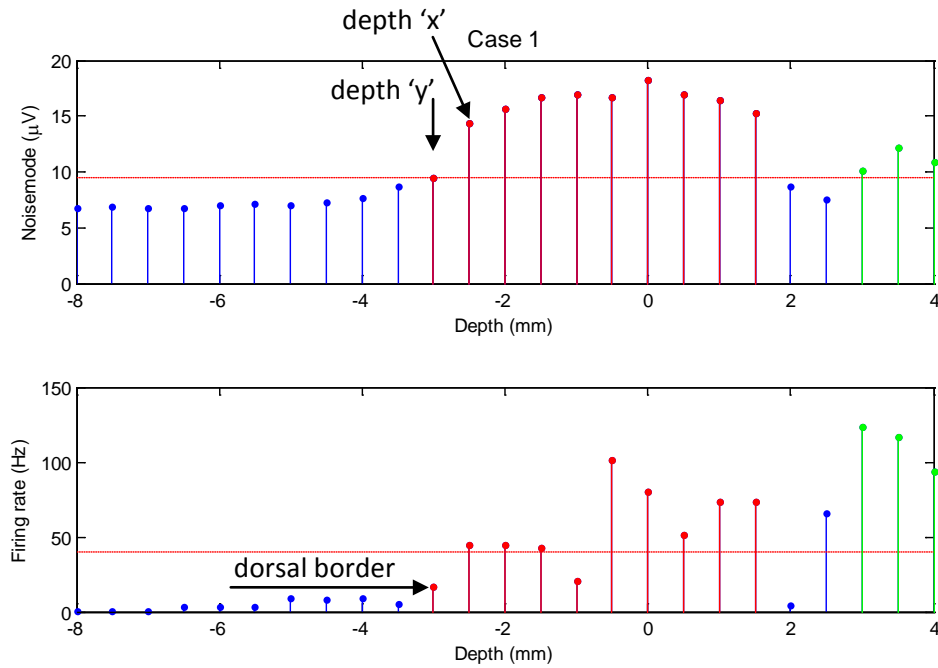
Figure 4.2b STN detection (dorsal border). For depth 'y', the firing rate was already below its threshold. Depths in red and blue were the annotated STN and SN area from our automated algorithm.

About the annotation of the ventral border of STN, from depth 'x', we searched forward and annotated the depth before it went back below the noisemode threshold. (Figure 4.3)
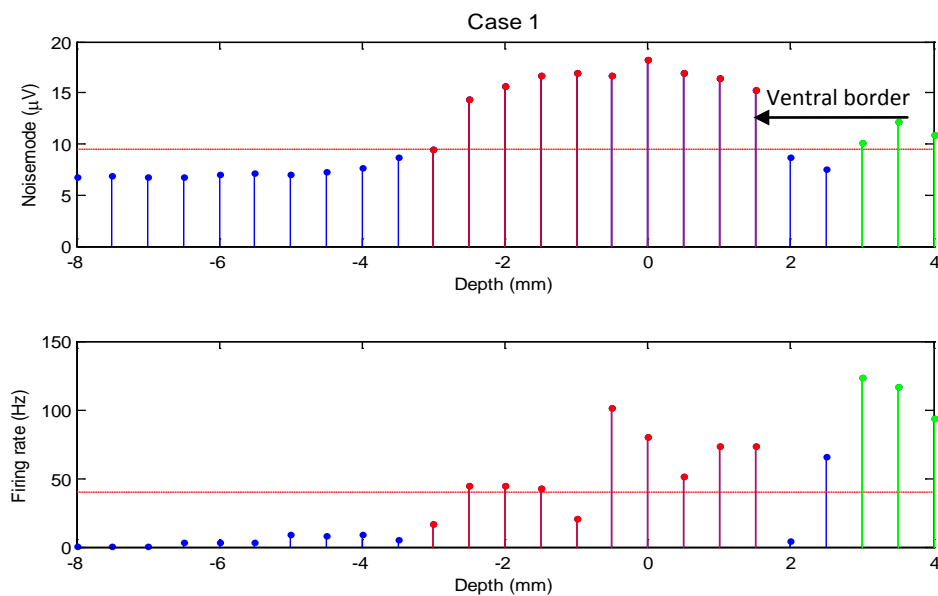

Figure 4.3 STN detection (ventral border). The annotation of the ventral border of STN was only depended on noisemode.

The other case for STN targeting was that no depth survived from noisemode threshold but some depths exceeded the firing rate threshold. We first checked the consecutiveness of the depths that exceeded the firing rate threshold. If there was only one cluster, then all these depths in that cluster were marked as STN. If there was more than one cluster, we annotated STN area from the first depth in the first cluster till the last depth in the last cluster.
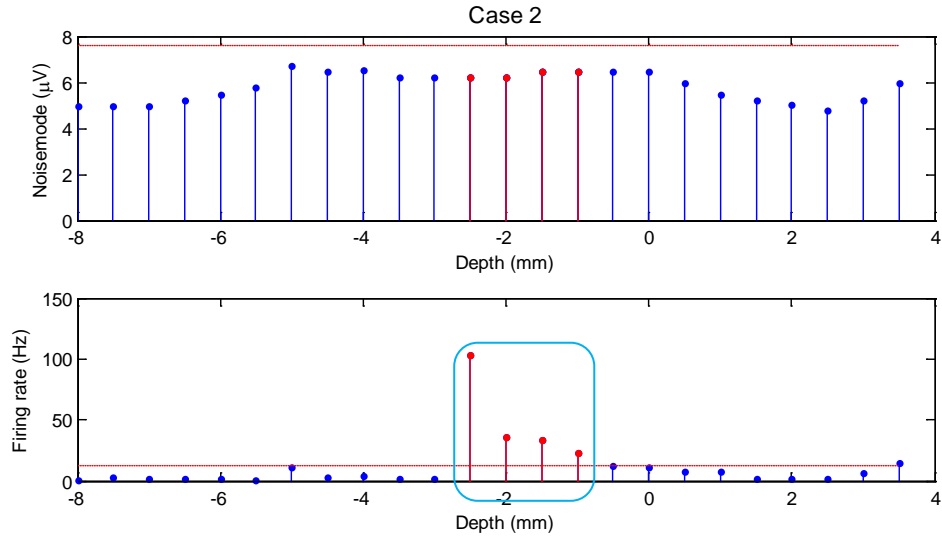
Figure 4.4 STN detection (1 cluster). For this dataset, no depth exceeded noisemode threshold, but there was one cluster observed that exceeded firing rate threshold.
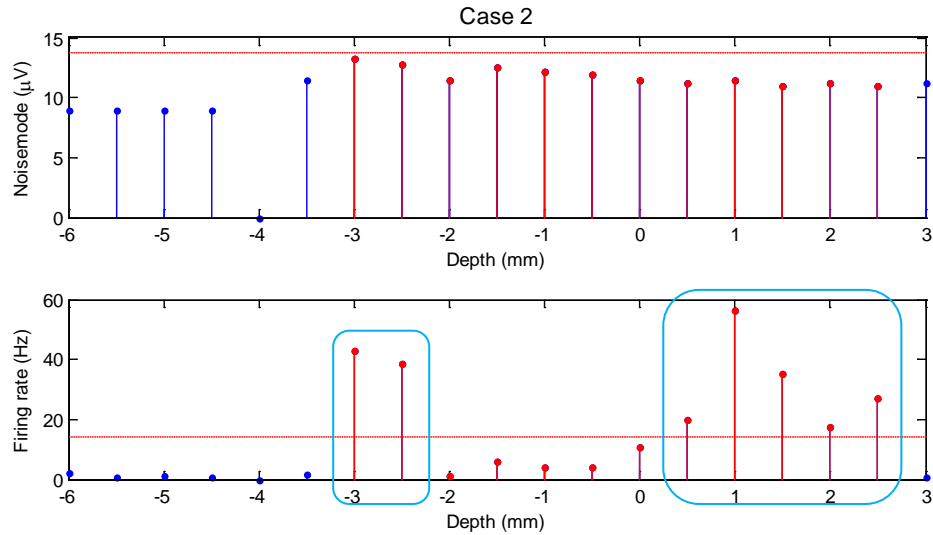

Figure 4.5 STN detection (>1 cluster). If more than one cluster exceeded firing rate threshold, the STN annotation was start from the first depth of the first cluster till the last depth of the last cluster.

It should be noted that we were searching for the clusters that exceeded the firing rate threshold. Therefore, if there was just single depth exceeded the threshold but not consecutive depths, we would ignore it and considered it as random fluctuation. Also for this case 2, only firing rate was used for target localization, so the confidence level of our annotation was not as high as the case 1 when both noisemode and firing rate exceeded their thresholds.

4.2 Nucleus SN Locating Algorithm

Because of the confidence level issue, SN targeting only applied to case 1. From ventral border of STN, the algorithm continued searching forward for the increasing slope of noisemode after it dropped below its threshold. When the increasing slope observed, we then checked the firing rate threshold to see whether dense neuronal discharge rate was obtained as well. If yes, those depths would be annotated as SN area. One assumption of our algorithm was that there was at least one depth gap between STN and SN. (The noisemode value for the gap depth should be below the noisemode threshold). If no gap observed, SN would not be annotated and probably the remaining depths would be annotated as STN as well.
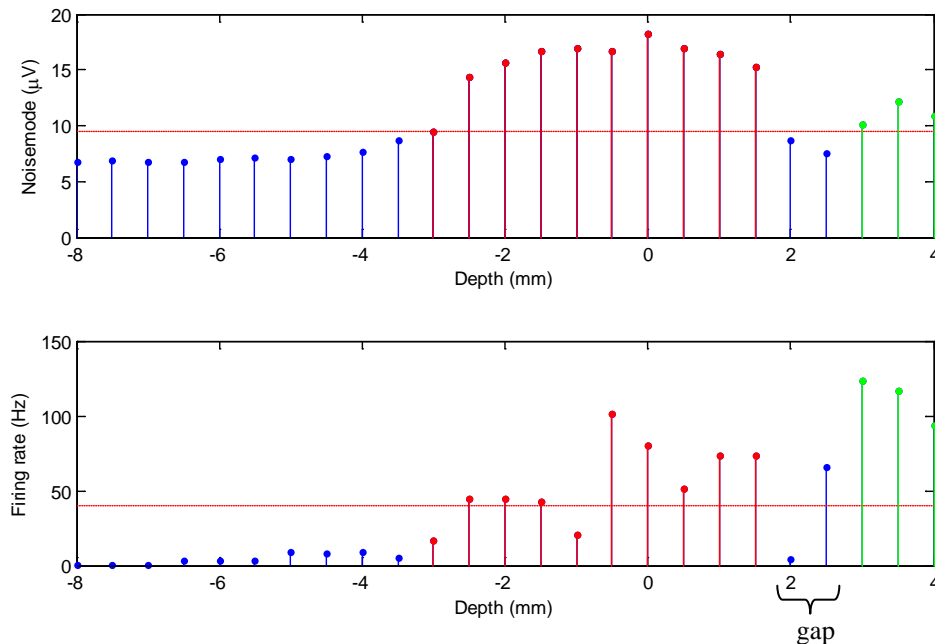

Figure 4.6 SN detection. Depth +2.5mm and +3.0mm were the gap between STN & SN. The noisemode increased again from depth +3.5mm and stayed above the noisemode threshold. Besides,

the values of firing rate for depth +3.0mm to depth +4.0mm were above the threshold. Therefore, depth +3.0mm to depth +4.0mm were annotated as SN.

4.3 Resulting Algorithm Analysis

The results of the targeting algorithm was analized in the following way. The algorithm for STN and SN detection was first applied to 14 trainning datasets to obtain the automated annotations. Figure 4.7 is one example of resulting annotation: For this dataset, the annotated STN area from our automated algorithm was from depth -2.5mm to +3.0mm. And there was no depth annotated as SN.
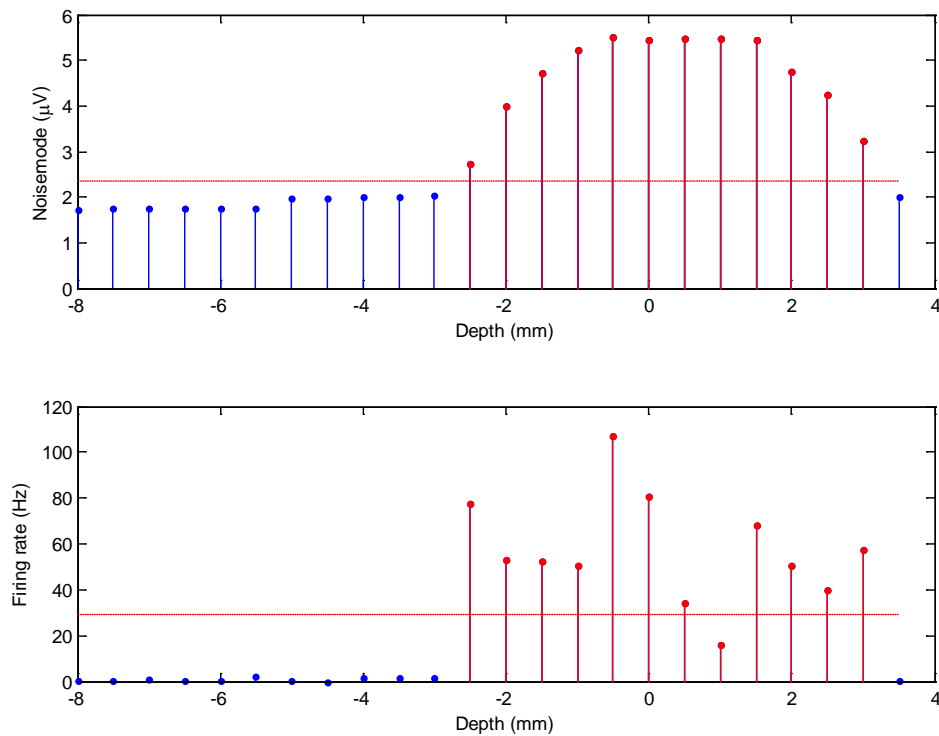
Figure 4.7 Resulting annotation. Here shows one example of the resulting annotation from automated target localization algorithm. Depths -2.5mm to +3.0mm were annotated as STN because of the high noisemode and high firing rate.

The annotation result was then compared with the surgical team's annotations made during DBS surgery. Besides, two independent annotations made by two neurologists were also involved in annotation comparisons.

46
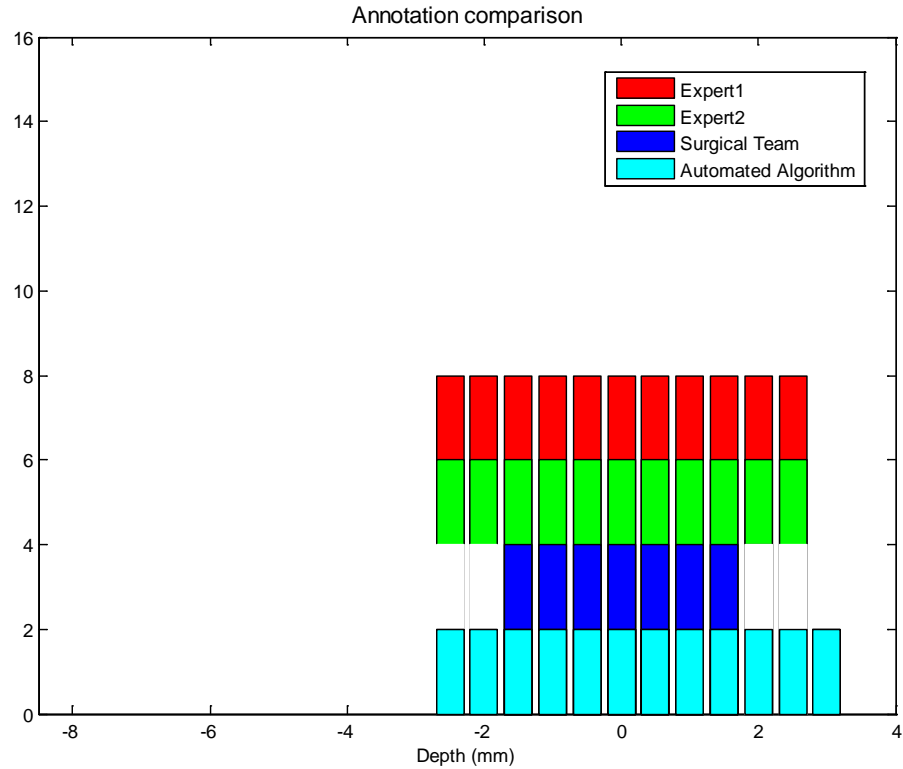
Figure 4.8 Annotation comparison. Red, green and blue bar were clinicians' annotation and the lowest cyan bar was our annotations. All clinicians' agreed that from depth -1.5mm to +2mm were the regions of STN. Two clinicians agreed with us that depths -2.5mm, -2mm and +2.5mm were also belong to STN area. But for depth +3mm, no clinician agreed it should be annotated as STN, so probably this depth should be considered as false positive.

Two neurologist only annotated the 14 training datasets to help us developing the automated targeting algorithm. Therefore, for the rest 70 datasets, the resulting annotations were only compared with the clinicians' annotation made during the surgery. Table 4-1 shows the agreement level of the resulting annotations.

Agreement Percentage	Surgical Team (84 datasets)	Expert 1 (14 training datasets)	Expert 2 (14 training datasets)
Automated Targeting	**89%**	**85%**	**88%**

Table 4-1 Annotation agreement percentage between automated targeting algorithm and clinicians

Additionally, the agreement percentage between these clinians' annotations were calculated as well. And the results are shown in Table 4-2.

Agreement Percentage	Expert 1 %	Expert 2 %
Surgical Team	87	88
Expert 2	89	

Table 4-2 Annotation Comparison between clinicians

For accurate localating the target nucleus, STN, the average deviation of border annotation was calculated. For both the dorsal border and ventral, the accuracy level were 0 ± 2 depths. (1 depth=0.5mm). This accuracy level was high so the result was quite satisfied.

Chapter 5 Conclusion & Future Work

As the main conclusion, the objective of this thesis work has been achieved, which was to develop an automated target localization algorithm for assisting neurologist to make fast and reliable annotation.

About the procedure of the study, first of all, the most robust noise level estimator was developed. With the accurate estimation of noise level, it was possible for the next crucial task of separating the MER signal into the components: background noise, spike and artifact. The information of background noise and spikes play an important role in target localization, since the annotations made by neurologists are mainly dependant on the characteristics of these two signals. Next, 15 statistical features are extract from the MER trace for distinguishing different signal characteristics. The noisemode, which can indicate the changes for target nuclei, and compound firing rate that changes according to the density of neural activities were chosen for developing the targeting algorithm for their consistent good performance. Threshold detection was applied to both features to achieve the highest agreement percentage with neurologists' annotation. After applying the resulting automated algorithm to all datasets, a high agreement level was achieved and the accuracy level of targeting the border of the target nucleus STN was also high.

It is still a tricky problem to distinguish different firing patterns for real MER signals for the fact that multiple units fire simultaneously, so it could be one possible topic for future work. With multiple units separated, the signal characteristics of firing pattern for one single unit would behave more close to the theoretical cases. And it would be particularly useful for distinguishing tonic and burst firing for two target nuclei STN & SN.

References

[1] Parkinson's disease, Wikipedia, http://en.wikipedia.org/wiki/Parkinson%27s_disease

[2] Eric R. Kandel, James H. Schwartz and Thomas M. Jessell. 2000. Principles of Neural Science (Fourth Edition). McGraw- Hill. p 853-865.

[3] The Basal Ganglia, http://www.dana.org/news/brainwork/detail.aspx?id=6028

[4] Elliot S. Krames, P. Hunter Peckham and Ali R. Rezai, Neuromodulation, Academic Press, Chapter 41-42 (p529-548), 2009

[5] A Raz, E Vaadia, H Bergman, Firing Patterns and Correlations of Spontaneous Discharge of Pallidal Neurons in the Normal and the Tremulous 1-Methyl-4-Phenyl-1,2,3,6-Tetrahydropyridine Vervet Model of Parkinsonism, J. Neurosci., 2000

[6] Deep Brain Stimulation, http://www.sciencedaily.com/releases/2008/06/080626144441.htm

[7] Anatomical terms of location, Wikipedia, http://en.wikipedia.org/wiki/Anatomical_terms_of_location

[8] Kevin Dolan, H.C.F. Martens, P.R. Schuurman, L.J. Bour, Automatic noise-level detection for extra-cellular micro-electrode recordings, J. Med BiolEng Comput, 2009

[9] MATLAB R2009b, The MathWorks, Natick, Massachusetts, United States

[10] S Wong, GH Baltuch, JL Jaggi, SF Danish, Functional Localization and Visualization of the Subthalamic Nucleus from Microelectrode Recordings Acquired During DBS Surgery With Unsupervised Machine Learning, J. Neural Eng., 2009

[11] PA Tass, Stochastic Phase Resetting of Two Coupled Phase Oscillators Stimulated at Different Times, J. Phys. Rev. E., 2003

[12] CR Legendy, M Salcman, Bursts and Recurrences of Bursts in the Spike Trains of Spontaneously Active Striate Cortex Neurons, J. Neurophysiol., 1985